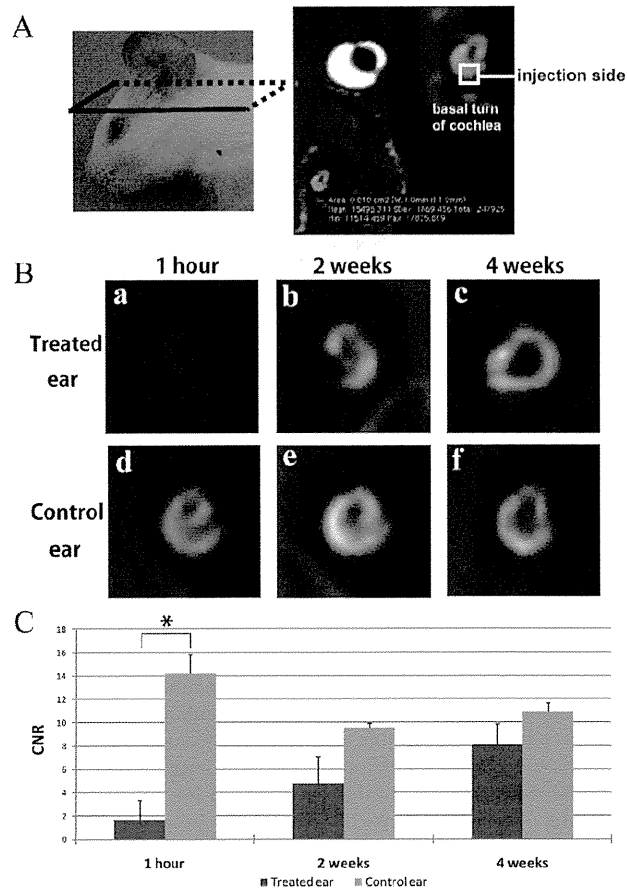

Fig. 3. *In vivo* MR images of cochlea. (A) MR image showing a slice parallel to the major axis of the guinea pig. (B) *In vivo* MR images of cochlea containing SPIO-labeled MSCs (treated ear; a–c) and untreated cochlea (control ear; d–f). The images were taken 1 h (a, d); 2 weeks (b, e); and 4 weeks after transplantation (c, f). (C) Bar graph comparing contrast-to-noise ratios (CNR) of treated and control ears over time. One hour after transplantation, the CNR of the treated ear was significantly lower ($P < 0.05$) than that of the control ear.

3. Results

3.1. Cell labeling

Prussian blue staining of SPIO-labeled MSCs showed that MSCs efficiently took up iron, as manifested by the many blue granules in the cells' cytoplasm (Fig. 1A and B). TEM of SPIO-labeled MSCs revealed the presence of numerous vesicles that were filled with electron-dense iron particles (Fig. 1C and D).

3.2. MR relaxometry

While T2 relaxation times of unlabeled MSCs (control) did not change with each cell concentration, T2 relaxation times of SPIO-labeled MSCs decreased in a dose-dependent manner (Fig. 2A). MR images of SPIO-labeled MSCs displayed low SI levels with cell concentrations over 5×10^6 cells/mL. Further examination confirmed that SI levels decreased with increasing cell concentrations (Fig. 2B).

3.3. In vivo MRI

The structure of the cochleae was clearly visualized with 1.5 T MRI (Fig. 3A). Images of areas that received saline injections displayed no hypointensity; these images were comparable to those of untreated ears (control) (Fig. 3A). By contrast, images of SPIO-labeled ears exhibited dramatic changes in SI as time progressed. One hour after transplantation, nearly the entire cochlea exhibited very low SI, similar to that obtained with MR images of *in vitro* samples containing 1×10^7 cells/mL (Figs. 2B and 3B). Two weeks after transplantation, SI tended to return to pre-transplantation levels. However, the SI of the injection site remained at a low intensity. Finally, 4 weeks after transplantation, SI was completely restored to pre-transplantation levels. The transplanted area no longer displayed low intensity signals. The mean CNRs for transplanted ears were 1.70 ± 1.64, 4.79 ± 2.25, and 8.04 ± 1.81 at 1 h, 2 weeks, and 4 weeks, respectively. On the other hand, the mean CNRs for non-transplanted ears were 14.19 ± 1.65, 9.52 ± 0.43, and 10.92 ± 0.75, respectively.

With regard to CNR, 1 h after transplantation the CNR of transplanted ears (treated ears) was significantly lower ($P < 0.05$) than that of non-transplanted ears (control ears) (Fig. 3B).

3.4. Histological analysis

One hour after transplantation, a large cluster of Prussian blue-positive cells was observed in the scala tympani of the basal turn (Fig. 4B). Four weeks after transplantation, however, only a few stained cells were found in the scala tympani (Fig. 4C). Some positive cells were found within the modiolus bony structure (Fig. 4E). In addition, the structures of all the cochleae of treated ears appeared normal and showed no obvious signs of disruption.

Fig. 5A shows a cell mass observed in scala tympani that was observed 1 h after transplantation. This mass was found to contain Iba-1 positive cells (Fig. 5B and C). Histological assessment of the cell mass 2 weeks after transplantation showed that the size of the mass had decreased (Fig. 5D).

4. Discussion

In this study, we labeled MSCs with SPIO *in vitro*, transplanted them into the inner ear, and monitored the labeled cells in the cochleae of living animals using MRI. This is the first study to demonstrate that local transplantation of labeled stem cells into the inner ear can be visualized *in vivo via* MRI. According to the CNR measurements, the SI of transplanted areas exhibited a low signal that differed significantly to that of non-transplanted ears, as soon as 1 h after transplantation. Also, MRI clearly visualized the transplants as areas of hypointensity. Two weeks after transplantation, the SI of transplanted areas tended to return to pre-transplantation levels, with SI levels completely reaching pre-injection levels 4 weeks after transplantation. These findings are similar to those obtained with an animal model for acute myocardial infarction (AMI) that received SPIO-labeled MSCs transplants into the heart myocardium (Peng et al., 2011). In the AMI study, serial tracking by MRI demonstrated that hypointensities remained 3 weeks after transplantation and that SI gradually returned to pre-implantation levels (Peng et al., 2011). Moreover, as with the present study, Peng and colleagues also observed limitations in transplant detection and in SI restoration as time progressed. These similarities could be due to decreases in the number of transplanted MSCs containing SPIO particles, which influence changes in the magnetic field. There are two possible explanations for this decrease in SPIO-labeled cells: cell division and phagocytosis by cochlear macrophages.

When considering cell division, the state of SPIO-labeled MSCs must be taken into account. It is generally known that the incorporation of SPIO particles into cells occurs through endosomal processes and through ingestion by lysosomes (Arbab et al., 2005; Matuszewski et al., 2005; Hsiao et al., 2007; Kiessling, 2008). Through these actions, SPIO particles are internalized and thereby accumulate in lysosomes in the cells. According to Arbab et al.,

Please cite this article in press as: Watada, Y., et al., Magnetic resonance monitoring of superparamagnetic iron oxide (SPIO)-labeled stem cells transplanted into the inner ear. Neurosci. Res. (2015), http://dx.doi.org/10.1016/j.neures.2015.01.010

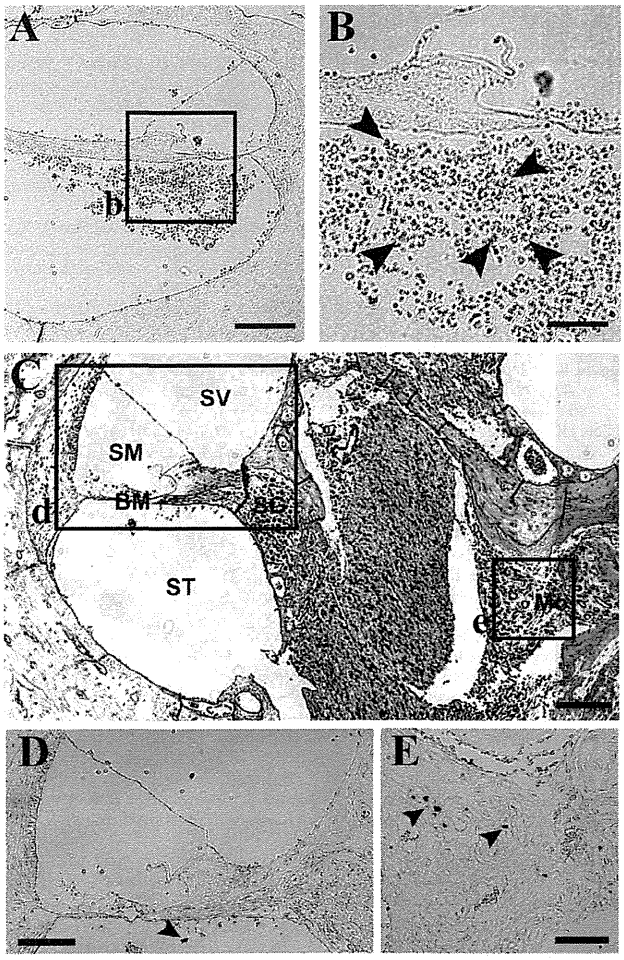

Fig. 4. Histological findings. (A) Prussian blue-stained section of a cochlea 1 h after transplantation with SPIO-labeled MSCs. Magnified images of the insets (b) are shown in B. (B) A block of Prussian blue-stained MSCs (arrowheads) localized to the basal turn. (C) Representative section of a cochlea 4 weeks after transplantation. This section was stained with H&E. D and E were stained with Prussian blue. Magnified images of the insets (d and e) are shown in D and E, respectively. BM, basement membrane; SG, spiral ganglion; SV, scala vestibular; SM, scala media; ST, scala tympani; Mo, modiolus. (D and E) Higher magnification images showing Prussian blue-positive cells (arrowheads) in the organ of Corti, including in the scala tympani (D), and the modiolus (E). Scale bars: A, 100 μm; B, 40 μm; C, 100 μm; D, 65 μm; E, 40 μm.

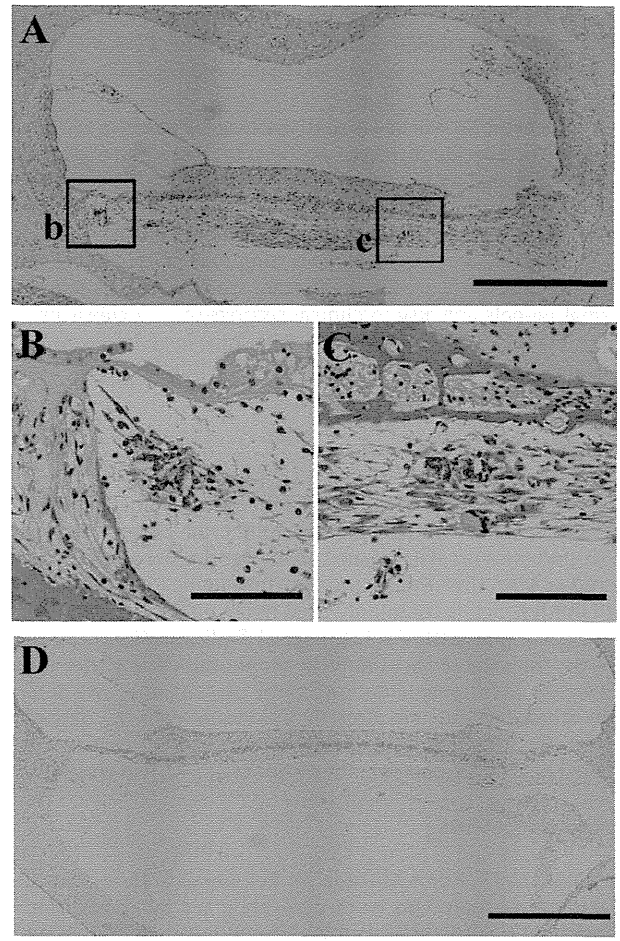

Fig. 5. Histological findings. (A) Prussian blue-stained section of a cochlea 1 day after transplantation with SPIO-labeled MSCs. Panels (B) and (C) are shown in the adjacent section. (B) and (C) Iba-1-stained section of the same area shown in insets (b) and (c) of panel (A). (D) Prussian blue-stained section of a cochlea 2 weeks after transplantation. Scale bars: A, 500 μm; B, 100 μm; C, 100 μm; D, 500 μm.

intracellular SPIO particles in rapidly dividing cells disappear from the cells within 2–3 weeks (Arbab et al., 2003), suggesting that MSCs retain SPIO particles for only a few weeks.

Phagocytosis by cochlear macrophages may also contribute to the decrease in SPIO-labeled MSCs that occurs with time. A small number of cochlear macrophages are known to exist predominantly in the spiral ligament and spiral ganglion. The number of cochlear macrophages immediately increases in response to damage—such as noise exposure, local surgical stress, and aminoglycoside ototoxity—as a result of macrophage migration from the vasculature to the cochlea (Okano et al., 2008; Hirose et al., 2005; Sato et al., 2008). Macrophages have been reported to reach the area of maximal damage between 1 and 4 days after delivery of a noise stimulus. There, they appear to phagocytize degenerating hair cells. Macrophages have been observed in these regions for 12–16 days (Warchol, 1997).

To determine whether macrophages contributed to the decrease in SPIO-labeled MSCs in the cochlea, cochlear sections were stained for the macrophage marker Iba-1 1 day and 2 weeks after transplantation. Okano et al. (2008) observed that the number of cochlear macrophages increased from 1 to 7 days and decreased to baseline after 4 weeks in response to cochlear damage. This is consistent with our observation of numerous Iba-1 positive macrophages in the cochlea in the vicinity of the transplant 1 day after transplantation (Fig. 5B and C). We suspect that the transplanted cells were phagocytized by cochlear macrophages attracted to the transplantation site. Two weeks later SPIO-labeled cells had disappeared, suggesting the possibility that SPIO-labeled cells had been phagocytized by the macrophages.

In addition, MRI revealed that this decrease in the number of labeled cells was accompanied by an increase in SI. Consequently as time progressed, SI gradually returned to pre-transplantation levels. Thus, MRI monitoring of SPIO-labeled transplanted cells may be limited to 2 weeks or to the length of time transplanted cells retain SPIO particles.

With regard to the transplanted area, just 1 h after transplantation we observed labeled cells attached to the scala tympani of the basal turn. Four weeks after transplantation, we observed a few cells in the scala tympani and the modiolus, suggesting the possibility that the cells migrated. Indeed, direct injection of stem cell transplants into the scala tympani results in migration from the scala tympani to and around the spiral ganglion, scala media, modiolus, and surrounding areas (Bogaerts et al., 2008; Coleman et al.,

Please cite this article in press as: Watada, Y., et al., Magnetic resonance monitoring of superparamagnetic iron oxide (SPIO)-labeled stem cells transplanted into the inner ear. Neurosci. Res. (2015), http://dx.doi.org/10.1016/j.neures.2015.01.010

2006; Hildebrand et al., 2005; Hu et al., 2005). Our results suggested that SPIO-labeled stem cells migrated for 4 weeks. However in this study, we did not examine whether the stem cells did indeed migrate.

Further studies will be needed. Histological analysis verified the presence of iron-positive cells in the area of the inner ear we targeted. We found a direct surgical approach to scala tympani to be the most ideal for local application of MSCs, in terms of reducing inflammatory tissue response and surgical difficulty (Kanzaki et al., 2007; Backhouse et al., 2008). This surgery is not technically difficult. The procedure used in the present study is well established in animal models and also in clinical settings (*e.g.*, cochlear implant surgery). The present study and its findings have implications for tracking transplanted SPIO-labeled MSCs in humans by MRI, which is a minimally invasive method.

5. Conclusions

Our results demonstrated that MSCs can be efficiently labeled *in vitro* using a commercially available and clinically approved SPIO preparation. SPIO-labeled MSCs can be detected and monitored *in vivo* after transplantation into guinea pig cochlea with 1.5T-MRI, which is commonly used in hospitals. The MRI findings were consistent with the histological findings. With both methods, the transplanted area could be monitored shortly after surgery (<2 weeks after transplantation). In the present study, we detected SPIO-labeled MSCs soon after transplantation. To the best of our knowledge, this is the first study to successfully visualize SPIO-labeled MSCs transplanted into the inner ear with *in vivo* MRI.

Acknowledgments

We thank Dr. Kunio Mizutari for helping with the optimization of data acquisition. This work was supported by grants from the Ministry of Health, Labor, and Welfare in Japan (H16-008OK) and Grant-in-Aid for Scientific Research (C) (No. 23592482 to D.Y) from the Ministry of Education, Culture, Sports, Science, and Technology of Japan (MEXT).

References

Amsalem, Y., Mardor, Y., Feinberg, M.S., Landa, N., Miller, L., Daniels, D., Ocherashvilli, A., Holbova, R., Yosef, O., Barbash, I.M., Leor, J., 2007. Iron-oxide labeling and outcome of transplanted mesenchymal stem cells in the infarcted myocardium. Circulation 116, I38–I45.

Arbab, A.S., Bashaw, L.A., Miller, B.R., Jordan, E.K., Lewis, B.K., Kalish, H., Frank, J.A., 2003. Characterization of biophysical and metabolic properties of cells labeled with superparamagnetic iron oxide nanoparticles and transfection agent for cellular MR imaging. Radiology 229, 838–846.

Arbab, A.S., Wilson, L.B., Ashari, P., Jordan, E.K., Lewis, B.K., Frank, J.A., 2005. A model of lysosomal metabolism of dextran coated superparamagnetic iron oxide (SPIO) nanoparticles: implications for cellular magnetic resonance imaging. NMR Biomed. 18, 383–389.

Backhouse, S., Coleman, B., Shepherd, R., 2008. Surgical access to the mammalian cochlea for cell-based therapies. Exp. Neurol. 214, 193–200.

Bogaerts, S., Douglas, S., Corlette, T., Pau, H., Saunders, D., Mckay, S., Oleskevich, S., 2008. Microsurgical access for cell injection into the mammalian cochlea. J. Neurosci. Methods 168, 156–163.

Bulte, J.W., Kraitchman, D.L., 2004. Iron oxide MR contrast agents for molecular and cellular imaging. NMR Biomed. 17, 484–499.

Cicchetti, F., Gross, R.E., Bulte, J.W., Owen, M., Chen, I., Saint-Pierre, M., Wang, X., Yu, M., Brownell, A.L., 2007. Dual-modality in vivo monitoring of subventricular zone stem cell migration and metabolism. Contrast Media Mol Imag 2, 130–138.

Coleman, B., Hardman, J., Coco, A., Epp, S., De Silva, M., Crook, J., Shepherd, R., 2006. Fate of embryonic stem cells transplanted into the deafened mammalian cochlea. Cell Transplant. 15, 369–380.

Cotanche, D.A., Kaiser, C.L., 2010. Hair cell fate decisions in cochlear development and regeneration. Hear. Res. 266, 18–25.

Farrell, E., Wielopolski, P., Pavljasevic, P., Van Tiel, S., Jahr, H., Verhaar, J., Weinans, H., Krestin, G., O'brien, F.J., Van Osch, G., Bernsen, M., 2008. Effects of iron oxide incorporation for long term cell tracking on MSC differentiation in vitro and in vivo. Biochem. Biophys. Res. Commun. 369, 1076–1081.

Geraerts, M., Verfaillie, C.M., 2009. Adult stem and progenitor cells. Adv. Biochem. Eng. Biotechnol. 114, 1–21.

Groves, A.K., 2010. The challenge of hair cell regeneration. Exp. Biol. Med. (Maywood) 235, 434–446.

Guo, J., Shen, J.K., Wang, L., Xiao, L., Zhang, R.J., Luo, W.F., Gong, Z.G., Sun, J., Xu, H., Sirois, P., Li, K., 2011. In vivo evaluation of cerebral transplantation of resovist-labeled bone marrow stromal cells in Parkinson's disease rats using magnetic resonance imaging. Appl. Biochem. Biotechnol. 163, 636–648.

Hildebrand, M.S., Dahl, H.H., Hardman, J., Coleman, B., Shepherd, R.K., De Silva, M.G., 2005. Survival of partially differentiated mouse embryonic stem cells in the scala media of the guinea pig cochlea. J. Assoc. Res. Otolaryngol. 6, 341–354.

Hirose, K., Discolo, C.M., Keasler, J.R., Ransohoff, R., 2005. Mononuclear phagocytes migrate into the murine cochlea after acoustic trauma. J. Comp. Neurol. 489, 180–194.

Hsiao, J.K., Tai, M.F., Chu, H.H., Chen, S.T., Li, H., Lai, D.M., Hsieh, S.T., Wang, J.L., Liu, H.M., 2007. Magnetic nanoparticle labeling of mesenchymal stem cells without transfection agent: cellular behavior and capability of detection with clinical 1.5 T magnetic resonance at the single cell level. Magn. Reson. Med. 58, 717–724.

Hu, Z., Wei, D., Johansson, C.B., Holmstrom, N., Duan, M., Frisen, J., Ulfendahl, M., 2005. Survival and neural differentiation of adult neural stem cells transplanted into the mature inner ear. Exp. Cell Res. 302, 40–47.

Jeon, S.J., Oshima, K., Heller, S., Edge, A.S., 2007. Bone marrow mesenchymal stem cells are progenitors in vitro for inner ear hair cells. Mol. Cell. Neurosci. 34, 59–68.

Jiang, Y., Jahagirdar, B.N., Reinhardt, R.L., Schwartz, R.E., Keene, C.D., Ortiz-Gonzalez, X.R., Reyes, M., Lenvik, T., Lund, T., Blackstad, M., Du, J., Aldrich, S., Lisberg, A., Low, W.C., Largaespada, D.A., Verfaillie, C.M., 2002. Pluripotency of mesenchymal stem cells derived from adult marrow. Nature 418, 41–49.

Kamiya, K., Fujinami, Y., Hoya, N., Okamoto, Y., Kouike, H., Komatsuzaki, R., Kusano, R., Nakagawa, S., Satoh, H., Fujii, M., Matsunaga, T., 2007. Mesenchymal stem cell transplantation accelerates hearing recovery through the repair of injured cochlear fibrocytes. Am. J. Pathol. 171, 214–226.

Kanzaki, S., Shiotani, A., Inoue, M., Hasegawa, M., Ogawa, K., 2007. Sendai virus vector-mediated transgene expression in the cochlea in vivo. Audiol. Neurootol. 12, 119–126.

Kiessling, F., 2008. Noninvasive cell tracking. Handb. Exp. Pharmacol., 305–321.

Matuszewski, L., Persigehl, T., Wall, A., Schwindt, W., Tombach, B., Fobker, M., Poremba, C., Ebert, W., Heindel, W., Bremer, C., 2005. Cell tagging with clinically approved iron oxides: feasibility and effect of lipofection, particle size, and surface coating on labeling efficiency. Radiology 235, 155–161.

Meyer, A.K., Maisel, M., Hermann, A., Stirl, K., Storch, A., 2010. Restorative approaches in Parkinson's disease: which cell type wins the race? J. Neurol. Sci. 289, 93–103.

Mori, T., Kiyono, T., Imabayashi, H., Takeda, Y., Tsuchiya, K., Miyoshi, S., Makino, H., Matsumoto, K., Saito, H., Ogawa, S., Sakamoto, M., Hata, J., Umezawa, A., 2005. Combination of hTERT and bmi-1, E6, or E7 induces prolongation of the life span of bone marrow stromal cells from an elderly donor without affecting their neurogenic potential. Mol. Cell. Biol. 25, 5183–5195.

Okano, T., Nakagawa, T., Kita, T., Kada, S., Yoshimoto, M., Nakahata, T., Ito, J., 2008. Bone marrow-derived cells expressing Iba1 are constitutively present as resident tissue macrophages in the mouse cochlea. J. Neurosci. Res. 86, 1758–1767.

Peng, C., Yang, K., Xiang, P., Zhang, C., Zou, L., Wu, X., Gao, Y., Kang, Z., He, K., Liu, J., Cheng, M., Wang, J., Chen, L., 2011. Effect of transplantation with autologous bone marrow stem cells on acute myocardial infarction. Int. J. Cardiol. 162, 158–165.

Pittenger, M.F., Mackay, A.M., Beck, S.C., Jaiswal, R.K., Douglas, R., Mosca, J.D., Moorman, M.A., Simonetti, D.W., Craig, S., Marshak, D.R., 1999. Multilineage potential of adult human mesenchymal stem cells. Science 284, 143–147.

Sato, E., Shick, H.E., Ransohoff, R.M., Hirose, K., 2008. Repopulation of cochlear macrophages in murine hematopoietic progenitor cell chimeras: the role of CX3CR1. J. Comp. Neurol. 506, 930–942.

Sykova, E., Jendelova, P., 2007. In vivo tracking of stem cells in brain and spinal cord injury. Prog. Brain Res. 161, 367–383.

Takeda, Y., Mori, T., Imabayashi, H., Kiyono, T., Gojo, S., Miyoshi, S., Hida, N., Ita, M., Segawa, K., Ogawa, S., Sakamoto, M., Nakamura, S., Umezawa, A., 2004. Can the life span of human marrow stromal cells be prolonged by bmi-1, E6, E7, and/or telomerase without affecting cardiomyogenic differentiation? J. Gene Med. 6, 833–845.

Warchol, M.E., 1997. Macrophage activity in organ cultures of the avian cochlea: demonstration of a resident population and recruitment to sites of hair cell lesions. J. Neurobiol. 33, 724–734.

Please cite this article in press as: Watada, Y., et al., Magnetic resonance monitoring of superparamagnetic iron oxide (SPIO)-labeled stem cells transplanted into the inner ear. Neurosci. Res. (2015), http://dx.doi.org/10.1016/j.neures.2015.01.010

ARTICLE IN PRESS

Molecular and Cellular Endocrinology ■■ (2014) ■■–■■

Contents lists available at ScienceDirect

Molecular and Cellular Endocrinology

journal homepage: www.elsevier.com/locate/mce

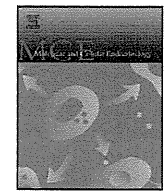

Review

Identification of novel steroidogenic factor 1 (SF-1)-target genes and components of the SF-1 nuclear complex

Tetsuya Mizutani [a,b,*], Shinya Kawabe [a,b], Shin Ishikane [a], Yoshitaka Imamichi [a,b], Akihiro Umezawa [c], Kaoru Miyamoto [a,b]

[a] Department of Biochemistry, Faculty of Medical Sciences, University of Fukui, Fukui 910-1193, Japan
[b] Translational Research Center, Organization for Life Science Advancement Programs, University of Fukui, Fukui 910-1193, Japan
[c] National Research Institute for Child Health and Development, Tokyo 157-8535, Japan

ARTICLE INFO

Article history:
Available online

Keywords:
Steroidogenesis
Transcriptional regulation
Glutathione S-transferase A family
5-aminolevulinic acid synthase 1
Ferredoxin reductase
CCAAT/enhancer-binding protein β

ABSTRACT

Steroidogenic factor 1 (SF-1) is a master regulator of adrenal and reproductive development and function. Although SF-1 was identified as a transcriptional regulator for steroid metabolic enzymes, it has been shown that SF-1 also regulates other genes that are involved in various cellular processes. Previously, we showed that introduction of SF-1 into mesenchymal stem cells resulted in the differentiation of these cells to the steroidogenic lineage. By using this method of differentiation, we performed comprehensive analyses to identify the novel SF-1-target genes and components of the SF-1 nuclear complex. Genome-wide analyses with promoter tiling array and DNA microarray identified 10 genes as novel SF-1-target genes including *glutathione S-transferase A* family, *5-aminolevulinic acid synthase 1* and *ferredoxin reductase*. Using SF-1 immuno-affinity chromatography of nuclear proteins followed by MS/MS analysis, we identified 24 proteins including CCAAT/enhancer-binding protein β as components of SF-1 nuclear complex. In this review, we will describe novel roles of the newly identified genes for steroidogenesis.

Contents

1. Introduction

Steroidogenic factor 1 (SF-1, also known as Ad4BP (adrenal 4-binding protein); encoded by *NR5A1* (nuclear receptor subfamily 5, group A, member 1)) plays a pivotal role in the regulation of reproductive and endocrine functions (Morohashi and Omura, 1996; Parker and Schimmer, 1997). SF-1 regulates the expression of steroidogenesis-related genes and is thus considered as a master regulator of steroid hormone production. Therefore, dysregulation of SF-1 and its target genes have been linked to diseases such as congenital steroid hormone deficiencies. Delineating the underlying molecular mechanisms of SF-1 functions may help in the understanding of congenital steroid hormone deficiencies with unknown causes and is important for the future development of therapeutic and diagnostic methods.

Mesenchymal stem cells (MSCs) have been shown to differentiate into not only mesodermal lineages such as adipocytes, chondrocytes and osteoblasts but also all three germ layers (Bianco et al., 2008). Previously, we reported that cAMP stimulation of cloned

Abbreviations: 3β-HSD, 3β-hydroxysteroid dehydrogenase; ALAS1, 5-aminolevulinic acid synthase 1; C/EBPβ, CCAAT/enhancer-binding protein β; 3C assay, chromosome conformation capture assay; FDXR, ferredoxin reductase; GSTA, glutathione S-transferase A; LRH-1, liver receptor homolog 1; MSCs, mesenchymal stem cells; PGC-1α, peroxisome proliferator-activated receptor-γ coactivator-1α; ROS, reactive oxygen species; SF-1, steroidogenic factor 1.

* Corresponding author. Department of Biochemistry, Faculty of Medical Sciences, University of Fukui, 23-3 Matsuokashimoaizuki, Eiheiji, Fukui 910-1193, Japan. Tel.: +81 776 61 8316; fax: +81 776 61 8102.
E-mail address: mizutani@u-fukui.ac.jp (T. Mizutani).

http://dx.doi.org/10.1016/j.mce.2014.11.019
0303-7207/

murine MSCs, KUM9, and human MSCs, hMSC-hTERT-E6/E7, stably expressing SF-1 induced cell differentiation into testicular Leydig-like and adrenocortical-like cells, respectively (Miyamoto et al., 2011; Yazawa et al., 2006). Similarly, adenovirus-mediated expression of SF-1 also differentiates primary bone marrow-derived and adipose tissue-derived MSCs into steroidogenic cells (Gondo et al., 2004, 2008; Tanaka et al., 2007). These results suggest that MSCs could be potentially used in cell and gene-based therapies for diseases related to steroid hormone production. Furthermore, these cells can be used as tools to analyze SF-1 functions, by examining changes in gene expressions and chromatin structure during the initial induction of the differentiation into steroidogenic cells by SF-1.

Identifying the target genes and components that constitute the nuclear transcription complex is critical in the understanding of transcription factor function. Using genome-wide analyses with promoter tiling array and DNA microarray, we identified 10 genes as novel SF-1-target genes including *glutathione S-transferase A* (*GSTA*) family (Matsumura et al., 2013), *5-aminolevulinic acid synthase 1* (*ALAS1*) (Ju et al., 2012) and *ferredoxin reductase* (*FDXR*) (Imamichi et al., 2014). We also identified 24 proteins, including CCAAT/enhancer-binding protein β (C/EBPβ), as components of the SF-1 nuclear complex (Mizutani et al., 2014) by SF-1 immuno-affinity chromatography of nuclear proteins followed by MS/MS analysis. In this review we describe results of comprehensive studies aimed at identifying novel SF-1-target genes and nuclear SF-1 complex components using differentiation-based methods. The novel roles of these newly identified genes in steroidogenesis are also described.

1.1. Novel SF-1-target genes and their transcriptional regulation

More than 40 genes have been identified as target genes of SF-1, including most steroidogenic enzymes (Schimmer and White, 2010). As mentioned earlier, we performed a combined analysis with promoter tiling array and DNA microarray using the differentiated cells, and identified 10 genes as novel SF-1-target genes (Ju et al., 2012). Recently, several groups also have performed genome-wide analyses to identify SF-1-target genes using mouse adrenocortical tumor Y1 cells or human adrenocortical H295R cells (Doghman et al., 2007; Ehrlund et al., 2012; Schimmer et al., 2011). Expression of many genes, which are involved in various functions other than steroidogenesis, were found to be directly or indirectly regulated by SF-1. Consistent with our results, *ALAS1*, *FDXR*, *CLU* and *UPP1* were also found as SF-1-regulated genes in Y1 cells (Schimmer et al., 2011), suggesting that expression of these genes were directly regulated by SF-1 in Y1 cells. Among the novel SF-1-target genes identified, we focused on three genes, *hGSTA3* (Matsumura et al., 2013), *ALAS1* (Ju et al., 2012) and *FDXR* (Imamichi et al., 2014) based on their transcriptional regulations.

1.2. Human glutathione S-transferase A3 (GSTA3)

Human *GSTA* genes (*hGSTA1–hGSTA4*) cluster on chromosome 6p12 (Hayes et al., 2005; Morel et al., 2002), all of which are regulated by SF-1. Curiously, however, only two of them (*hGSTA3* and *hGSTA4*) have SF-1 binding sites in their promoter regions. It suggests a chromatin-based alteration of gene structure that enables the coordinated expression of the clustered *hGSTA* genes. Chromosome conformation capture assay (3C assay) is an excellent method to analyze genomic interactions between genes that are separated by hundreds of megabases. The 3C assays revealed that the coordinated expression of *hGSTA* genes was based on changes in higher-order chromatin structure triggered by SF-1, which enabled the formation of long-range interactions (Fig. 1). Furthermore, SF-1 domain mapping indicated that the hinge region of SF-1 would be necessary for such long-range interactions. These results prompted us to speculate that certain nuclear factors may bind to the hinge region of SF-1 to alter chromosomal conformations that enabled *hGSTA* gene promoters to localize in closer proximity to the *hGSTA3* promoter.

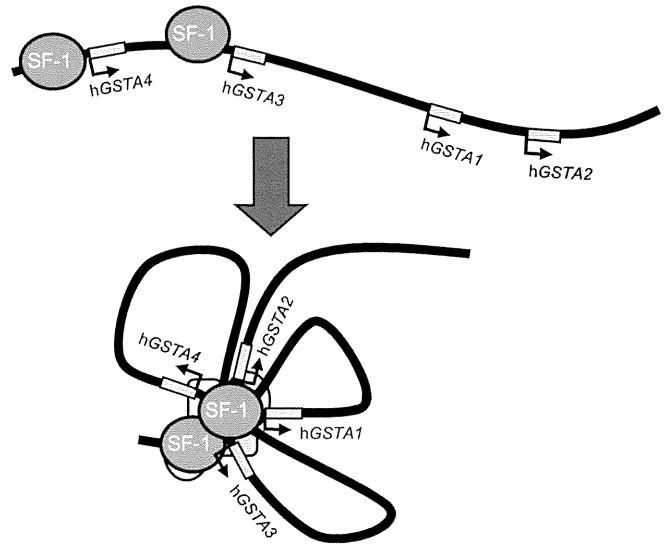

Fig. 1. Model of chromatin loop formation of *hGSTA* family genes via SF-1. SF-1 directly binds to the *hGSTA3* and *A4* promoters but not to the *A1* and *A2* promoters. Subsequently, SF-1 triggers higher-order chromatin conformational changes within the *hGSTA* family gene locus on chromosome 6p12 to cause induction of all *hGSTA* family gene expressions.

A primary role of GSTs is the detoxification of electrophilic compounds. On the other hand, steroid double-bond isomerase activities have been reported for bacterially expressed recombinant hGSTA1-1 and hGSTA3-3 proteins (Johansson and Mannervik, 2001). However, in living cells, it is not clear whether or not GSTA family proteins are involved in steroidogenesis. Currently, dehydrogenation of the 3-hydroxy group and subsequent Δ^5–Δ^4 isomerization of steroid hormone precursors in steroidogenesis are thought to be enzymatic properties of 3β-hydroxysteroid dehydrogenase (3β-HSD) (Payne and Hales, 2004; Simard et al., 2005). In our study, hGSTA1-1 and hGSTA3-3 represent novel members of steroidogenic enzymes, which participate in Δ^5–Δ^4 isomerization of steroid hormone precursors in a cooperative fashion with 3β-HSD, as schematically shown in Fig. 2. Mutations or deletions of *3β-HSD* can cause congenital disorders related to steroidogenesis. Therefore it is possible that deletions or mutations of *hGSTA1* or *hGSTA3* may be a causative factor in these disorders, although our preliminary search could identify neither mutations nor deletions of these genes. Further analysis is clearly needed to clarify whether abnormalities of *hGSTA* family could cause any congenital disorders related to steroidogenesis.

To date, none of the rodent *GSTA* homologs has been reported to have the isomerase activity. Therefore effects of mutations or deletions of these genes on steroid hormone production can only be examined in humans. Interestingly, expression of several transcripts encoding the mu family of murine *GSTs* have been shown to be regulated by SF-1 (Schimmer et al., 2011). The mu family of murine *GSTs* might be the counterpart of *hGSTA* family.

Although hGSTA2-2 and hGSTA4-4 are not directly related to steroidogenesis, their gene expressions are under the control of SF-1. It has been reported that reactive oxygen species (ROS), such as superoxide, is accumulated by gonadotropin in Leydig cells and granulosa cells and function in Erk1/2 signaling and ovulation, respectively (Tai and Ascoli, 2011; Yacobi et al., 2007). ROS also has been considered to be an aging-related inhibitor of testosterone

Please cite this article in press as: Tetsuya Mizutani, et al., Identification of novel steroidogenic factor 1 (SF-1)-target genes and components of the SF-1 nuclear complex, Molecular and Cellular Endocrinology (2014), doi: 10.1016/j.mce.2014.11.019

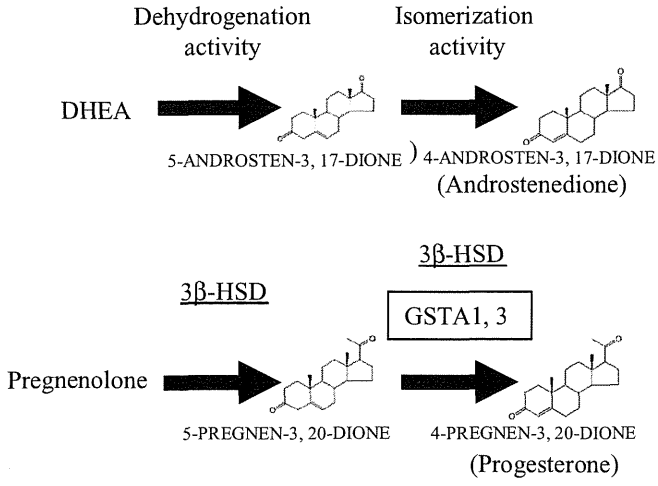

Fig. 2. Role of hGSTA1-1 and A3-3 in steroidogenesis. Human 3β-HSD II is known to have two enzymatic activities, dehydrogenation of the 3-hydroxy group and subsequent Δ^5–Δ^4 isomerization. In addition to 3β-HSD II, GSTA1-1 and A3-3 function cooperatively to catalyze Δ^5–Δ^4 isomerization to produce progesterone or Δ^4-androstenedione in steroidogenic cells.

synthesis in Leydig cell (Midzak et al., 2009). GSTA family proteins might contribute to regulate ROS concentration in these cells.

1.3. 5-aminolevulinic acid synthase 1 (ALAS1) and ferredoxin reductase (FDXR)

ALAS1 and *FDXR* were also identified as novel SF-1-target genes. ALAS catalyzes a reaction between glycine and succinyl-CoA to form 5-aminolevulinic acid. ALAS1 participates in heme synthesis for all cytochrome family proteins in various tissues, including P450 enzymes in steroidogenic pathways (May et al., 1995). Because heme is essential for the catalytic activities of P450 enzymes, ALAS1 is expected to be involved in steroid metabolism. FDXR is a flavoprotein localized in mitochondrial inner membrane that transfers electrons from NADPH to cytochrome P450 enzymes, mediated by ferredoxins (Miller, 2005; Sheftel et al., 2010; Shi et al., 2012). The electron transfer system is involved in various metabolic processes, including the synthesis of bile acid, iron–sulfur clusters, vitamin D, and steroid hormones (Miller and Bose, 2011; Shi et al., 2012; Vickery, 1997). *ALAS1* and *FDXR* are ubiquitously expressed in various tissues but are particularly highly expressed in steroidogenic tissues, such as the adrenals and gonads (Brentano et al., 1992; Okano et al., 2010). We demonstrated that *ALAS1* and *FDXR* expression in steroidogenic cells were enhanced by SF-1 through its binding to the 3.5-kb upstream and the intronic regions, respectively. *ALAS1*, but not *FDXR*, is also highly expressed in the liver, suggesting involvement of the enzyme in drug metabolism in the liver (Okano et al., 2010). Interestingly, peroxisome proliferator-activated receptor-γ coactivator-1α (PGC-1α) works as a co-activator for *ALAS1* gene expression in both steroidogenic tissues and the liver. PGC-1α is a key regulator of metabolic processes in various tissues such as skeletal muscle, fat and liver (Lin et al., 2005). PGC-1α also works together with SF-1 (and liver receptor homolog 1 (LRH-1) which is another member of NR5A family) as a co-activator, which markedly enhances the expression of its target genes in the ovary (Yazawa et al., 2010). As for in the liver, in spite of the presence of LRH-1, it has been reported that PGC-1α augments *ALAS1* gene expression via co-activation of forkhead box protein O1 and nuclear respiratory factor-1 transcription factors bound to the promoter region (Handschin et al., 2005). Unlike in the liver, we demonstrated that PGC-1α strongly augments *ALAS1* gene expression caused by SF-1 binding to the 3.5-kb upstream region in the steroidogenic cells as illustrated in Fig. 3. Although *ALAS1* is one of the housekeeping genes, it may be controlled in a tissue-specific manner, particularly in steroidogenic tissues by SF-1 (and LRH-1).

2. Nuclear complex of SF-1

Transcription factors recognize and bind to their target sequences and form a complex with a number of specific nuclear proteins. Therefore, it is critical to identify the components of a nuclear complex of a certain transcription factor to elucidate its transcriptional regulatory mechanism. It has been reported that SF-1 directly interacts with numerous factors including coactivators, corepressors and other transcription factors (Schimmer and White, 2010). PGC-1α directly interacts with SF-1 via a LXXLL-related motif. Dosage-sensitive sex reversal-adrenal hypoplasia congenital critical region on the X chromosome, gene 1, also contains this motif to bind SF-1 at the same region (Kawajiri et al., 2003; Yazawa et al., 2010). Expression levels and nuclear localizations of both proteins might affect the SF-1-mediated transcriptional regulation of its target genes. Theoretically, SF-1 would form large complexes with various proteins to facilitate appropriate gene expression patterns. However, isolation and characterization of such SF-1 nuclear complexes from nuclear extracts have not been reported to date. Using nuclear extracts prepared from differentiated MSCs under mild conditions (under physiological ionic strength) that enable isolation of native SF-1 complex, we performed SF-1 immunoaffinity chromatography followed by MS/MS analysis (Mizutani et al., 2014). We identified 24 proteins including transcription-related proteins as well as DNA repair factors and splicing factors. Consistent with this result, Wang et al. reported that SF-1 works together with the DNA repair proteins Ku70/80 as a regulator of centrosome homoeostasis, but not in the nucleus (Wang et al., 2013). These results suggest that SF-1 would work for the various functions in addition to the transcriptional regulation.

C/EBPβ was also identified as a component of the SF-1 nuclear protein complex. C/EBPβ is known as an essential transcription factor for ovulation and luteinization in the ovary. Targeted disruption of the *Cebpb* gene caused infertility in female mice, as a result of ovulation and luteinization failure (Sterneck et al., 1997). Granulosa cell-specific conditional knockout studies revealed that expression of C/EBPβ is induced by luteinizing hormone (LH) and activated in an

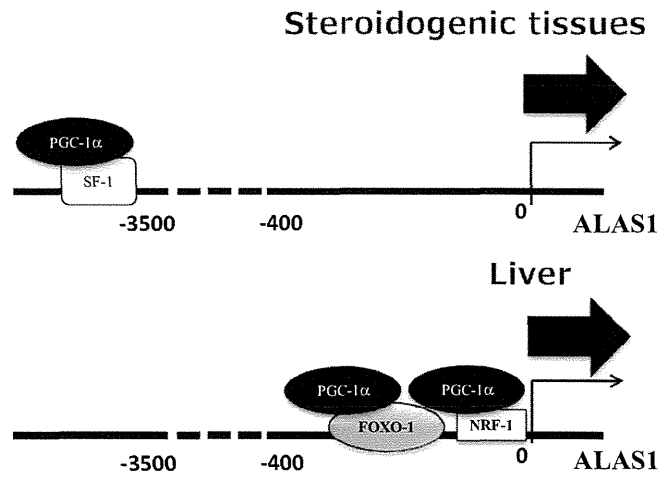

Fig. 3. Different transcriptional regulations of *ALAS1* between steroidogenic cells and liver. Schematic drawing of distinct transcriptional regulations of *ALAS1* in steroidogenic cells and liver.

Please cite this article in press as: Tetsuya Mizutani, et al., Identification of novel steroidogenic factor 1 (SF-1)-target genes and components of the SF-1 nuclear complex, Molecular and Cellular Endocrinology (2014), doi: 10.1016/j.mce.2014.11.019

extracellular signal-regulated kinase 1/2-dependent manner in preovulatory follicles (Fan et al., 2009). Moreover, analysis of *Cebpa/b*$^{gc-/-}$ double-mutant mice revealed that C/EBPα is also involved in this process (Fan et al., 2011). As for coordinated actions of C/EBPs with SF-1, the effects of C/EBPβ on *STAR* gene expression in several species are well documented (Christenson et al., 1999; Reinhart et al., 1999; Silverman et al., 1999, 2006; Tremblay et al., 2002). However, such coordinated actions of C/EBPβ on other genes have not been well reported. In our study, it was shown that C/EBPβ knockdown attenuated the cAMP-induced progesterone production in granulosa tumor-derived KGN cells through altering gene expression of *STAR* as well as *CYP11A1* and *HSD3B2*. The observation may be responsible for the facts that C/EBP proteins were bound to the human *STAR, CYP11A1* and *HSD3B2* gene upstream regions that may contribute to the expression of these genes. Collectively C/EBPβ is an important mediator of progesterone production by working together with SF-1 (and also LRH-1) to activate *STAR, CYP11A1* and *HSD3B2* genes, especially under tropic hormone-stimulated conditions.

3. Conclusion

SF-1 is an essential regulator of reproductive and endocrine functions, including expression of steroidogenesis-related genes. Recently, in addition to steroid metabolic enzymes, several accessory factors (e.g. detoxification enzymes or those related to electron transfer, heme biosynthesis etc.) were also identified as SF-1-target genes. Thus, SF-1 would participate in the regulation of most, if not all, genes related to steroidogenesis. The identification of some housekeeping genes such as *ALAS1* or *FDXR* as SF-1 targets, and the recent reports describing glycolytic enzyme genes as SF-1 targets (Baba et al., 2014) and the involvement of SF-1 in centromere homeostasis (Lai et al., 2011; Wang et al., 2013) suggest wider roles of SF-1 in the body apart from steroidogenesis regulation. Since ALAS1 and FDXR are known to be involved in the energy metabolic pathway other than steroidogenesis, ALAS1 and FDXR may also be involved in the pathway for development of steroidogenic tissues. Further study may reveal such diverse functions of SF-1.

Acknowledgements

This work was supported by a grant from the Ministry of Education, Culture, Sports, Science and Culture; and a Health and Labour Sciences Research grant from the Ministry of Health, Labour and Welfare; Research on Development of New Drugs; and the Smoking Research Foundation.

References

Baba, T., Otake, H., Sato, T., Miyabayashi, K., Shishido, Y., Wang, C.Y., et al., 2014. Glycolytic genes are targets of the nuclear receptor Ad4BP/SF-1. Nat. Commun. 5, 3634.

Bianco, P., Robey, P.G., Simmons, P.J., 2008. Mesenchymal stem cells: revisiting history, concepts, and assays. Cell Stem Cell 2, 313–319.

Brentano, S.T., Black, S.M., Lin, D., Miller, W.L., 1992. cAMP post-transcriptionally diminishes the abundance of adrenodoxin reductase mRNA. Proc. Natl. Acad. Sci. U.S.A. 89, 4099–4103.

Christenson, L.K., Johnson, P.F., McAllister, J.M., Strauss, J.F., 1999. CCAAT/enhancer-binding proteins regulate expression of the human steroidogenic acute regulatory protein (StAR) gene. J. Biol. Chem. 274, 26591–26598.

Doghman, M., Karpova, T., Rodrigues, G.A., Arhatte, M., De Moura, J., Cavalli, L.R., et al., 2007. Increased steroidogenic factor-1 dosage triggers adrenocortical cell proliferation and cancer. Mol. Endocrinol. 21, 2968–2987.

Ehrlund, A., Jonsson, P., Vedin, L.L., Williams, C., Gustafsson, J., Treuter, E., 2012. Knockdown of SF-1 and RNF31 affects components of steroidogenesis, TGFβ, and Wnt/β-catenin signaling in adrenocortical carcinoma cells. PLoS ONE 7, e32080.

Fan, H.Y., Liu, Z., Shimada, M., Sterneck, E., Johnson, P.F., Hedrick, S.M., et al., 2009. MAPK3/1 (ERK1/2) in ovarian granulosa cells are essential for female fertility. Science 324, 938–941.

Fan, H.Y., Liu, Z., Johnson, P.F., Richards, J.S., 2011. CCAAT/enhancer-binding proteins (C/EBP)-α and -β are essential for ovulation, luteinization, and the expression of key target genes. Mol. Endocrinol. 25, 253–268.

Gondo, S., Yanase, T., Okabe, T., Tanaka, T., Morinaga, H., Nomura, M., et al., 2004. SF-1/Ad4BP transforms primary long-term cultured bone marrow cells into ACTH-responsive steroidogenic cells. Genes Cells 9, 1239–1247.

Gondo, S., Okabe, T., Tanaka, T., Morinaga, H., Nomura, M., Takayanagi, R., et al., 2008. Adipose tissue-derived and bone marrow-derived mesenchymal cells develop into different lineage of steroidogenic cells by forced expression of steroidogenic factor 1. Endocrinology 149, 4717–4725.

Handschin, C., Lin, J., Rhee, J., Peyer, A.K., Chin, S., Wu, P.H., et al., 2005. Nutritional regulation of hepatic heme biosynthesis and porphyria through PGC-1alpha. Cell 122, 505–515.

Hayes, J.D., Flanagan, J.U., Jowsey, I.R., 2005. Glutathione transferases. Annu. Rev. Pharmacol. Toxicol. 45, 51–88.

Imamichi, Y., Mizutani, T., Ju, Y., Matsumura, T., Kawabe, S., Kanno, M., et al., 2014. Transcriptional regulation of human ferredoxin reductase through an intronic enhancer in steroidogenic cells. Biochim. Biophys. Acta 1839, 33–42.

Johansson, A.S., Mannervik, B., 2001. Human glutathione transferase A3-3, a highly efficient catalyst of double-bond isomerization in the biosynthetic pathway of steroid hormones. J. Biol. Chem. 276, 33061–33065.

Ju, Y., Mizutani, T., Imamichi, Y., Yazawa, T., Matsumura, T., Kawabe, S., et al., 2012. Nuclear receptor 5A (NR5A) family regulates 5-aminolevulinic acid synthase 1 (ALAS1) gene expression in steroidogenic cells. Endocrinology 153, 5522–5534.

Kawajiri, K., Ikuta, T., Suzuki, T., Kusaka, M., Muramatsu, M., Fujieda, K., et al., 2003. Role of the LXXLL-motif and activation function 2 domain in subcellular localization of Dax-1 (dosage-sensitive sex reversal-adrenal hypoplasia congenita critical region on the X chromosome, gene 1). Mol. Endocrinol. 17, 994–1004.

Lai, P.Y., Wang, C.Y., Chen, W.Y., Kao, Y.H., Tsai, H.M., Tachibana, T., et al., 2011. Steroidogenic factor 1 (NR5A1) resides in centrosomes and maintains genomic stability by controlling centrosome homeostasis. Cell Death Differ. 18, 1836–1844.

Lin, J., Handschin, C., Spiegelman, B.M., 2005. Metabolic control through the PGC-1 family of transcription coactivators. Cell Metab. 1, 361–370.

Matsumura, T., Imamichi, Y., Mizutani, T., Ju, Y., Yazawa, T., Kawabe, S., et al., 2013. Human glutathione S-transferase A (GSTA) family genes are regulated by steroidogenic factor 1 (SF-1) and are involved in steroidogenesis. FASEB J. 27, 3198–3208.

May, B.K., Dogra, S.C., Sadlon, T.J., Bhasker, C.R., Cox, T.C., Bottomley, S.S., 1995. Molecular regulation of heme biosynthesis in higher vertebrates. Prog. Nucleic Acid Res. Mol. Biol. 51, 1–51.

Midzak, A.S., Chen, H., Papadopoulos, V., Zirkin, B.R., 2009. Leydig cell aging and the mechanisms of reduced testosterone synthesis. Mol. Cell. Endocrinol. 299, 23–31.

Miller, W.L., 2005. Minireview: regulation of steroidogenesis by electron transfer. Endocrinology 146, 2544–2550.

Miller, W.L., Bose, H.S., 2011. Early steps in steroidogenesis: intracellular cholesterol trafficking. J. Lipid Res. 52, 2111–2135.

Miyamoto, K., Yazawa, T., Mizutani, T., Imamichi, Y., Kawabe, S.Y., Kanno, M., et al., 2011. Stem cell differentiation into steroidogenic cell lineages by NR5A family. Mol. Cell. Endocrinol. 336, 123–126.

Mizutani, T., Ju, Y., Imamichi, Y., Osaki, T., Yazawa, T., Kawabe, S., et al., 2014. C/EBPbeta (CCAAT/enhancer-binding protein beta) mediates progesterone production through transcriptional regulation in co-operation with SF-1 (steroidogenic factor-1). Biochem. J. 460, 459–471.

Morel, F., Rauch, C., Coles, B., Le Ferrec, E., Guillouzo, A., 2002. The human glutathione transferase alpha locus: genomic organization of the gene cluster and functional characterization of the genetic polymorphism in the hGSTA1 promoter. Pharmacogenetics 12, 277–286.

Morohashi, K.I., Omura, T., 1996. Ad4BP/SF-1, a transcription factor essential for the transcription of steroidogenic cytochrome P450 genes and for the establishment of the reproductive function. FASEB J. 10, 1569–1577.

Okano, S., Zhou, L., Kusaka, T., Shibata, K., Shimizu, K., Gao, X., et al., 2010. Indispensable function for embryogenesis, expression and regulation of the nonspecific form of the 5-aminolevulinate synthase gene in mouse. Genes Cells 15, 77–89.

Parker, K.L., Schimmer, B.P., 1997. Steroidogenic factor 1: a key determinant of endocrine development and function. Endocr. Rev. 18, 361–377.

Payne, A.H., Hales, D.B., 2004. Overview of steroidogenic enzymes in the pathway from cholesterol to active steroid hormones. Endocr. Rev. 25, 947–970.

Reinhart, A.J., Williams, S.C., Clark, B.J., Stocco, D.M., 1999. SF-1 (steroidogenic factor-1) and C/EBP beta (CCAAT/enhancer binding protein-beta) cooperate to regulate the murine StAR (steroidogenic acute regulatory) promoter. Mol. Endocrinol. 13, 729–741.

Schimmer, B.P., White, P.C., 2010. Minireview: steroidogenic factor 1: its roles in differentiation, development, and disease. Mol. Endocrinol. 24, 1322–1337.

Schimmer, B.P., Tsao, J., Cordova, M., Mostafavi, S., Morris, Q., Scheys, J.O., 2011. Contributions of steroidogenic factor 1 to the transcription landscape of Y1 mouse adrenocortical tumor cells. Mol. Cell. Endocrinol. 336, 85–91.

Sheftel, A.D., Stehling, O., Pierik, A.J., Elsasser, H.P., Muhlenhoff, U., Webert, H., et al., 2010. Humans possess two mitochondrial ferredoxins, Fdx1 and Fdx2, with distinct roles in steroidogenesis, heme, and Fe/S cluster biosynthesis. Proc. Natl. Acad. Sci. U.S.A. 107, 11775–11780.

Shi, Y., Ghosh, M., Kovtunovych, G., Crooks, D.R., Rouault, T.A., 2012. Both human ferredoxins 1 and 2 and ferredoxin reductase are important for iron-sulfur cluster biogenesis. Biochim. Biophys. Acta 1823, 484–492.

Silverman, E., Eimerl, S., Orly, J., 1999. CCAAT enhancer-binding protein beta and GATA-4 binding regions within the promoter of the steroidogenic acute regulatory protein (StAR) gene are required for transcription in rat ovarian cells. J. Biol. Chem. 274, 17987–17996.

Please cite this article in press as: Tetsuya Mizutani, et al., Identification of novel steroidogenic factor 1 (SF-1)-target genes and components of the SF-1 nuclear complex, Molecular and Cellular Endocrinology (2014), doi: 10.1016/j.mce.2014.11.019

Silverman, E., Yivgi-Ohana, N., Sher, N., Bell, M., Eimerl, S., Orly, J., 2006. Transcriptional activation of the steroidogenic acute regulatory protein (StAR) gene: GATA-4 and CCAAT/enhancer-binding protein beta confer synergistic responsiveness in hormone-treated rat granulosa and HEK293 cell models. Mol. Cell. Endocrinol. 252, 92–101.

Simard, J., Ricketts, M.L., Gingras, S., Soucy, P., Feltus, F.A., Melner, M.H., 2005. Molecular biology of the 3beta-hydroxysteroid dehydrogenase/delta5-delta4 isomerase gene family. Endocr. Rev. 26, 525–582.

Sterneck, E., Tessarollo, L., Johnson, P.F., 1997. An essential role for C/EBPbeta in female reproduction. Genes Dev. 11, 2153–2162.

Tai, P., Ascoli, M., 2011. Reactive oxygen species (ROS) play a critical role in the cAMP-induced activation of Ras and the phosphorylation of ERK1/2 in Leydig cells. Mol. Endocrinol. 25, 885–893.

Tanaka, T., Gondo, S., Okabe, T., Ohe, K., Shirohzu, H., Morinaga, H., et al., 2007. Steroidogenic factor 1/adrenal 4 binding protein transforms human bone marrow mesenchymal cells into steroidogenic cells. J. Mol. Endocrinol. 39, 343–350.

Tremblay, J.J., Hamel, F., Viger, R.S., 2002. Protein kinase A-dependent cooperation between GATA and CCAAT/enhancer-binding protein transcription factors regulates steroidogenic acute regulatory protein promoter activity. Endocrinology 143, 3935–3945.

Vickery, L.E., 1997. Molecular recognition and electron transfer in mitochondrial steroid hydroxylase systems. Steroids 62, 124–127.

Wang, C.Y., Kao, Y.H., Lai, P.Y., Chen, W.Y., Chung, B.C., 2013. Steroidogenic factor 1 (NR5A1) maintains centrosome homeostasis in steroidogenic cells by restricting centrosomal DNA-dependent protein kinase activation. Mol. Cell. Biol. 33, 476–484.

Yacobi, K., Tsafriri, A., Gross, A., 2007. Luteinizing hormone-induced caspase activation in rat preovulatory follicles is coupled to mitochondrial steroidogenesis. Endocrinology 148, 1717–1726.

Yazawa, T., Mizutani, T., Yamada, K., Kawata, H., Sekiguchi, T., Yoshino, M., et al., 2006. Differentiation of adult stem cells derived from bone marrow stroma into Leydig or adrenocortical cells. Endocrinology 147, 4104–4111.

Yazawa, T., Inaoka, Y., Okada, R., Mizutani, T., Yamazaki, Y., Usami, Y., et al., 2010. PPAR-gamma coactivator-1alpha regulates progesterone production in ovarian granulosa cells with SF-1 and LRH-1. Mol. Endocrinol. 24, 485–496.

Please cite this article in press as: Tetsuya Mizutani, et al., Identification of novel steroidogenic factor 1 (SF-1)-target genes and components of the SF-1 nuclear complex, Molecular and Cellular Endocrinology (2014), doi: 10.1016/j.mce.2014.11.019

A calcium-dependent protease as a potential therapeutic target for Wolfram syndrome

Simin Lu[a,b], Kohsuke Kanekura[a], Takashi Hara[a], Jana Mahadevan[a], Larry D. Spears[a], Christine M. Oslowski[c], Rita Martinez[d], Mayu Yamazaki-Inoue[e], Masashi Toyoda[e], Amber Neilson[d], Patrick Blanner[d], Cris M. Brown[a], Clay F. Semenkovich[a], Bess A. Marshall[f], Tamara Hershey[g], Akihiro Umezawa[e], Peter A. Greer[h], and Fumihiko Urano[a,i,1]

[a]Department of Medicine, Division of Endocrinology, Metabolism, and Lipid Research, Washington University School of Medicine, St. Louis, MO 63110; [b]Graduate School of Biomedical Sciences, University of Massachusetts Medical School, Worcester, MA 01655; [c]Department of Medicine, Boston University School of Medicine, Boston, MA 02118; [d]Department of Genetics, iPSC core facility, Washington University School of Medicine, St. Louis, MO 63110; [e]Department of Reproductive Biology, National Center for Child Health and Development, Tokyo 157-8535, Japan; [f]Department of Pediatrics, Washington University School of Medicine, St. Louis, MO 63110; [g]Departments of Psychiatry, Neurology, and Radiology, Washington University School of Medicine, St. Louis, MO 63110; [h]Department of Pathology and Molecular Medicine, Queen's University, Division of Cancer Biology and Genetics, Queen's Cancer Research Institute, Kingston, Ontario K7L3N6, Canada; and [i]Department of Pathology and Immunology, Washington University School of Medicine, St. Louis, MO 63110

Edited by Stephen O'Rahilly, University of Cambridge, Cambridge, United Kingdom, and approved November 7, 2014 (received for review November 4, 2014)

Wolfram syndrome is a genetic disorder characterized by diabetes and neurodegeneration and considered as an endoplasmic reticulum (ER) disease. Despite the underlying importance of ER dysfunction in Wolfram syndrome and the identification of two causative genes, Wolfram syndrome 1 (*WFS1*) and Wolfram syndrome 2 (*WFS2*), a molecular mechanism linking the ER to death of neurons and β cells has not been elucidated. Here we implicate calpain 2 in the mechanism of cell death in Wolfram syndrome. Calpain 2 is negatively regulated by WFS2, and elevated activation of calpain 2 by WFS2-knockdown correlates with cell death. Calpain activation is also induced by high cytosolic calcium mediated by the loss of function of WFS1. Calpain hyperactivation is observed in the WFS1 knockout mouse as well as in neural progenitor cells derived from induced pluripotent stem (iPS) cells of Wolfram syndrome patients. A small-scale small-molecule screen targeting ER calcium homeostasis reveals that dantrolene can prevent cell death in neural progenitor cells derived from Wolfram syndrome iPS cells. Our results demonstrate that calpain and the pathway leading its activation provides potential therapeutic targets for Wolfram syndrome and other ER diseases.

Wolfram syndrome | endoplasmic reticulum | diabetes | neurodegeneration | treatment

The endoplasmic reticulum (ER) takes center stage for protein production, redox regulation, calcium homeostasis, and cell death (1, 2). It follows that genetic or acquired ER dysfunction can trigger a variety of common diseases, including neurodegenerative diseases, metabolic disorders, and inflammatory bowel disease (3, 4). Breakdown in ER function is also associated with genetic disorders such as Wolfram syndrome (5–8). It is challenging to determine the exact effects of ER dysfunction on the fate of affected cells in common diseases with polygenic and multifactorial etiologies. In contrast, we reasoned that it should be possible to define the role of ER dysfunction in mechanistically homogenous patient populations, especially in rare diseases with a monogenic basis, such as Wolfram syndrome (9).

Wolfram syndrome (OMIM 222300) is a rare autosomal recessive disorder characterized by juvenile-onset diabetes mellitus and bilateral optic atrophy (7). Insulin-dependent diabetes usually occurs as the initial manifestation during the first decade of life, whereas the diagnosis of Wolfram syndrome is invariably later, with onset of symptoms in the second and ensuing decades (7, 10, 11). Two causative genes for this genetic disorder have been identified and named Wolfram syndrome 1 (*WFS1*) and Wolfram syndrome 2 (*WFS2*) (12, 13). It has been shown that multiple mutations in the *WFS1* gene, as well as a specific mutation in the *WFS2* gene, lead to β cell death and neurodegeneration through ER and mitochondrial dysfunction (5, 6, 14–16). *WFS1* gene variants are also associated with a risk of type 2 diabetes (17). Moreover, a specific *WFS1* variant can cause autosomal dominant diabetes (18), raising the possibility that this rare disorder is relevant to common molecular mechanisms altered in diabetes and other human chronic diseases in which ER dysfunction is involved.

Despite the underlying importance of ER malfunction in Wolfram syndrome, and the identification of *WFS1* and *WFS2* genes, a molecular mechanism linking the ER to death of neurons and β cells has not been elucidated. Here we show that the calpain protease provides a mechanistic link between the ER and death of neurons and β cells in Wolfram syndrome.

Results

The causative genes for Wolfram syndrome, *WFS1* and *WFS2*, encode transmembrane proteins localized to the ER (5, 12, 13). Mutations in the *WFS1* or *WFS2* have been shown to induce neuronal and β cell death. To determine the cell death pathways emanating from the ER, we sought proteins associated with Wolfram syndrome causative gene products. HEK293 cells were transfected with a GST-tagged WFS2 expression plasmid. The GST-WFS2 protein was purified along with associated proteins on a glutathione affinity resin. These proteins were separated by

Significance

Wolfram syndrome is an autosomal recessive disorder characterized by juvenile diabetes and neurodegeneration, and is considered a prototype of human endoplasmic reticulum (ER) disease. Wolfram syndrome is caused by loss of function mutations of Wolfram syndrome 1 or Wolfram syndrome 2 genes, which encode transmembrane proteins localized to the ER. Despite its rarity, Wolfram syndrome represents the best human disease model currently available to identify drugs and biomarkers associated with ER health. Furthermore, this syndrome is ideal for studying the mechanisms of ER stress-mediated death of neurons and β cells. Here we report that the pathway leading to calpain activation offers potential drug targets for Wolfram syndrome and substrates for calpain might serve as biomarkers for this syndrome.

Author contributions: S.L., P.A.G., and F.U. designed research; S.L., K.K., T. Hara, J.M., L.D.S., C.M.O., R.M., M.Y.-I., M.T., A.N., P.B., and C.M.B. performed research; S.L., B.A.M., T. Hershey, A.U., and F.U. contributed new reagents/analytic tools; S.L., K.K., T. Hara, J.M., L.D.S., C.M.O., R.M., M.Y.-I., M.T., A.N., P.B., C.M.B., C.F.S., P.A.G., and F.U. analyzed data; and S.L., C.F.S., P.A.G., and F.U. wrote the paper.

The authors declare no conflict of interest.

This article is a PNAS Direct Submission.

Freely available online through the PNAS open access option.

[1]To whom correspondence should be addressed. Email: urano@dom.wustl.edu.

This article contains supporting information online at www.pnas.org/lookup/suppl/doi:10.1073/pnas.1421055111/-/DCSupplemental.

SDS/PAGE and visualized by Coomassie staining. Matrix-assisted laser desorption/ionization-time of flight (MALDI-TOF) mass spectroscopic analysis revealed 13 interacting proteins (Table S1), and one of the WFS2-associated polypeptides was CAPN2, the catalytic subunit of calpain 2, a member of the calcium dependent cysteine proteases family whose members mediate diverse biological functions including cell death (19–21) (Fig. 1*A*). Previous studies have shown that calpain 2 activation is regulated on the ER membrane and it plays a role in ER stress-induced apoptosis and β cell death (20, 22–24), which prompted us to study the role of WFS2 in calpain 2 activation.

Calpain 2 is a heterodimer consisting the CAPN2 catalytic subunit and the CAPNS1 (previously known as CAPN4) regulatory subunit. We first verified that WFS2 interacts with calpain 2 by showing that endogenous calpain 2 subunits CAPN2 (Fig. 1*B*) and CAPNS1 (Fig. 1*C*) each associated with GST-tagged WFS2 expressed in HEK293 cells. Endogenous CAPN2 was also found to be coimmunoprecipated with N- or C-terminal FLAG-tagged WFS2 expressed in HEK293 cells (Fig. S1 *A* and *B*, respectively). To further confirm these findings, we performed a coimmunoprecipitation experiment in Neuro2a cells (a mouse neuroblastoma cell line) and INS-1 832/13 cells (a rat pancreatic β cell line)

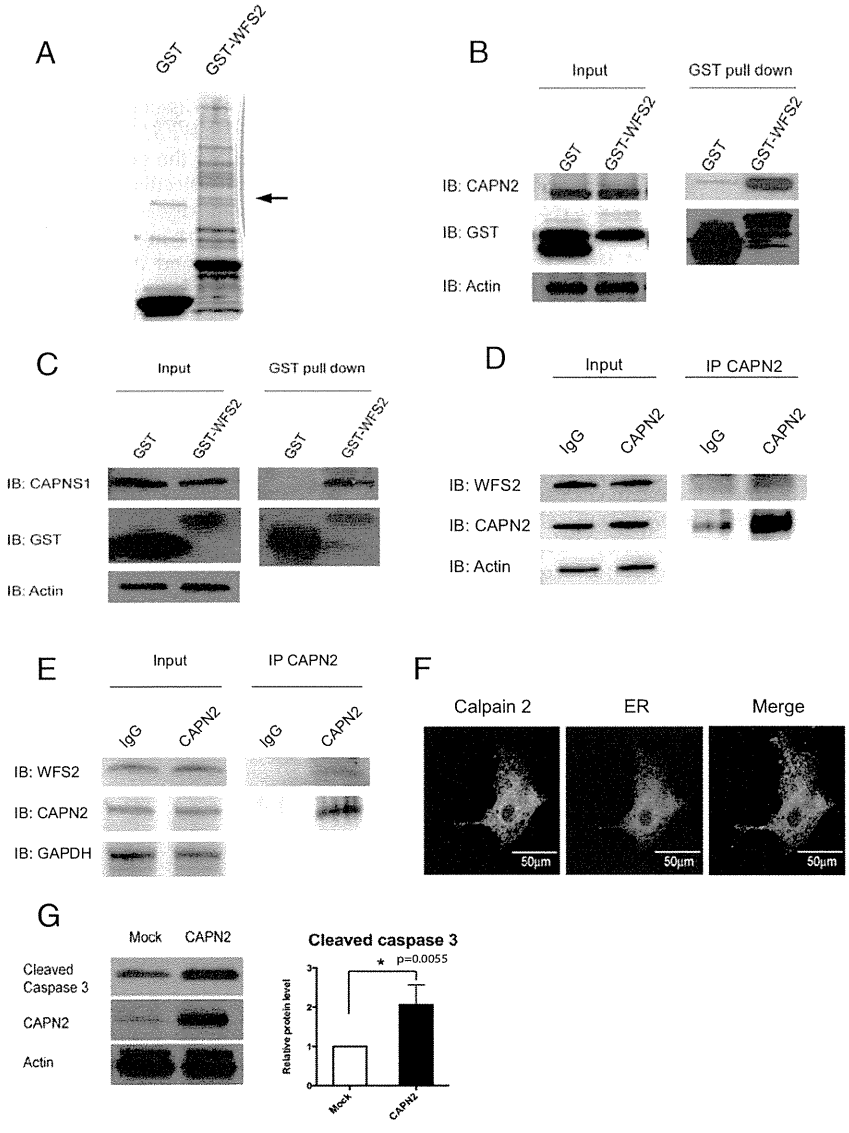

Fig. 1. WFS2 interacts with CAPN2. (*A*) Affinity purification of WFS2-associated proteins from HEK293 cells transfected with GST or GST-WFS2 expression plasmid. Proteins were separated by SDS/PAGE and visualized by Coomassie blue staining. CAPN2 was identified by MALDI-TOF analysis and denoted by an arrow. (*B*) GST-tagged WFS2 was pulled down on a glutathione affinity resin from lysates of HEK293 cells transfected with a GST-WFS2 expression plasmid, and the pulled-down products were analyzed for CAPN2 by immunoblotting with anti-CAPN2 antibody. (*C*) GST-tagged WFS2 was pulled down on a glutathione affinity resin from lysates of HEK293 cells transfected with GST-WFS2 expression plasmid and the pulled-down products were analyzed for CAPNS1 by immunoblotting with anti-CAPNS1 antibody. (*D*) Lysates of Neuro2a cells were immunoprecipitated with IgG or anti-calpain 2 antibodies. Lysates of IgG and anti-calpain 2 immunoprecipitates were analyzed for WFS2, CAPN2 or actin by immunoblotting. (*E*) Lysates of INS-1 832/13 cells were immunoprecipitated with IgG or anti-calpain 2 antibody. Lysates of IgG and anti-calpain 2 immunoprecipitates were analyzed for WFS2, CAPN2 or actin by immunoblotting. (*F*) COS7 cells were transfected with pDsRed2-ER vector (*Center*) and stained with anti-calpain 2 antibody (*Left*). (*Right*) A merged image is shown. (*G*) HEK293 cells were transfected with empty expression plasmid or a CAPN2 expression plasmid. Apoptosis was monitored by immunoblotting analysis of caspase 3 cleavage. (*Left*) Expression levels of CAPN2 and actin were measured by immunoblotting. (*Right*) Quantification of immunoblot is shown ($n = 3$, $^*P < 0.05$).

and found that endogenous WFS2 interacted with endogenous CAPN2 (Fig. 1 *D* and *E*). WFS2 is known to be a transmembrane protein localized to the ER. We therefore explored the possibility that calpain 2 might also localize to the ER. We transfected COS7 cells with pDsRed2-ER vector to visualize ER. Immunofluorescence staining of COS7 cells showed that endogenous calpain 2 was mainly localized to the cytosol, but also showed that a small portion colocalized with DsRed2-ER protein at the ER (Fig. 1*F*). Cell fractionation followed by immunoblot further confirmed this observation (Fig. S1*C*). Collectively, these results suggest that calpain 2 interacts with WFS2 at the cytosolic face of the ER.

Calpain hyperactivation has been shown to contribute to cell loss in various diseases (19), raising the possibility that calpain 2 might be involved in the regulation of cell death. To verify this issue, we overexpressed CAPN2, the catalytic subunit of calpain 2, and observed increase of cleaved caspase-3 in HEK293 cells indicating that hyperactivation of calpain 2 induces cell death (Fig. 1*G*).

To determine whether WFS2 plays a role in cell survival, we suppressed WFS2 expression in mouse neuronal NSC34 cells using siRNA and measured cell death under normal and ER stress conditions. WFS2 knockdown was associated with increased cleavage of caspase-3 in normal or ER stressed conditions (Fig. 2 *A* and *B*). We subsequently evaluated calpain 2 activation by measuring the cleavage of alpha II spectrin, a substrate for calpain 2. RNAi-mediated knockdown of WFS2 induced calpain activation, especially under ER stress conditions (Fig. 2*A*).

In patients with Wolfram syndrome, destruction of β cells leads to juvenile-onset diabetes (25). This finding prompted us to examine whether WFS2 was also involved in pancreatic β cell death. As was seen in neuronal cells, knockdown of WFS2 in rodent β cell lines INS1 832/13 (Fig. 2*C*) and MIN6 (Fig. S2) was also associated with increased caspase-3 cleavage under both normal and ER stress conditions. The association of WFS2 with calpain 2 and their involvement in cell viability suggested that calpain 2 activation might be the cause of cell death in WFS2-deficient cells. To further explore the relationship between WFS2 and calpain 2, we expressed WFS2 together with the calpain 2 catalytic subunit CAPN2 and measured apoptosis. Ectopic expression of WFS2 significantly suppressed calpain 2-associated apoptosis under normal and ER stress conditions (Fig. 2*D*, lane 4 and lane 8, and Fig. 2*E*). Next, we tested whether CAPN2 mediates cell death induced by WFS2 deficiency. When CAPN2 was silenced in WFS2-deficient cells, apoptosis was partially suppressed compared with untreated WFS2-deficient cells (Fig. 2*F*). Taken together, these results suggest that WFS2 is a negative regulator of calpain 2 proapoptotic functions.

To further confirm that loss of function of WFS2 leads to cell death mediated by calpain 2, we tested if calpeptin, a calpain inhibitor, could prevent cell death in WFS2-deficient cells. In agreement with previous observations, calpeptin treatment prevented WFS2-knockdown-mediated cell death in neuronal (Fig. 3 *A* and *B*) and β cell lines (Fig. 3*C* and Fig. S3*A*). Collectively, these results indicate that WFS2 is a suppressor of calpain 2-mediated cell death.

CAPN2 is the catalytic subunit of calpain 2. CAPN2 forms a heterodimer with the regulatory subunit, CAPNS1, which is required for protease activity and stability. We next explored the role of WFS2 in CAPN2 and CAPNS1 protein stability. Ectopic expression or RNAi-mediated knockdown of WFS2 did not correlate with changes in the steady-state expression of CAPN2 (Fig. S3*B*). By contrast, overexpression of WFS2 significantly reduced CAPNS1 protein expression (Fig. 3*D*) and transient suppression of WFS2 slightly increased CAPNS1 protein expression (Fig. 3*D*). These data suggest that WFS2 might be involved in CAPNS1 protein turnover, which is supported by the data showing that GST-tagged WFS2 expressed in HEK293 cells associated with endogenous CAPNS1 (Fig. 1*C*). To investigate whether WFS2 regulates CAPNS1 stability through the ubiquitin-proteasome pathway, we treated HEK293 cells ectopically expressing WFS2 with a proteasome inhibitor, MG132, and then measured CAPNS1 protein level. MG132 treatment stabilized CAPNS1 protein in cells ectopically expressing WFS2 (Fig. 3*E*). Furthermore, we performed cycloheximide chase experiments using HEK293 cells ectopically expressing WFS2 and quantified CAPNS1 protein levels at different time points. Ectopic expression of WFS2 was associated with significantly accelerated CAPNS1 protein loss, indicating that WFS2 contributes to posttranslational regulation of CAPNS1 (Fig. 3*F*). To further assess whether WFS2 is involved in the ubiquitination of CAPNS1, we measured the levels of CAPNS1 ubiquitination in cells ectopically expressing WFS2 and observed that CAPNS1 ubiquitination was increased by ectopic expression of WFS2 (Fig. 3*G*).

To further investigate the role of WFS2 in calpain 2 regulation, we collected brain lysates from WFS2 knockout mice. Measured levels of cleaved spectrin, a well characterized substrate for calpain (26). Notably, protein expression levels of cleaved spectrin, as well as CAPNS1, were significantly increased in WFS2 knockout mice compared with control mice (Fig. 3*H*). Collectively, these results indicate that WFS2 inhibits calpain 2 activation by regulating CAPNS1 degradation mediated by the ubiquitin-proteasome system.

Calpain 2 is a calcium-dependent protease. *WFS1*, the other causative gene for Wolfram syndrome, has been shown to be involved in calcium homeostasis (27, 28), suggesting that the loss of function of WFS1 may also cause calpain activation. To evaluate this possibility, we measured calpain activation levels in brain tissues from WFS1 brain-specific knockout and control mice. We observed a significant increase in a calpain-specific spectrin cleavage product, reflecting higher calpain activation levels in WFS1 knockout mice compared with control mice (Fig. 4*A*). The suppression levels of WFS1 in different parts of the brain were shown in Fig. 4*B*. To further confirm that calpain is activated by the loss of WFS1, we looked for other calpain substrates in brain tissues from WFS1 knockout mice using a proteomics approach. Two-dimensional fluorescence gel electrophoresis identified 12 proteins differentially expressed between cerebellums of WFS1 knockout mice and those of control mice (Fig. 4 *C* and *D*). Among these, myelin basic protein (MBP) is a known substrate for calpain in the brain (29). We measured myelin basic protein levels in brain lysates from WFS1 knockout and control mice. Indeed, the cleavage and degradation of myelin basic protein was increased in WFS1 knockout mice relative to control mice (Fig. 4*E*).

Next, we looked for evidence of increased calpain activity in Wolfram syndrome patient cells. We created neural progenitor cells derived from induced pluripotent stem cells (iPSCs) of Wolfram syndrome patients with mutations in *WFS1*. Fibroblasts from four unaffected controls and five patients with Wolfram syndrome were transduced with four reprogramming genes (Sox2, Oct4, c-Myc, and Klf4) (30) (Table S2). We produced at least 10 iPSC clones from each control and Wolfram patient. All control- and Wolfram-iPSCs, exhibited characteristic human embryonic stem cell morphology, expressed pluripotency markers including ALP, NANOG, SOX2, SSEA4, TRA-1–81, and had a normal karyotype (Fig. 5 *A–F*). To create neural progenitor cells, we first formed neural aggregates from iPSCs. Neural aggregates were harvested at day 5, replated onto new plates to give rise to colonies containing neural rosette structures. At day 12, neural rosette clusters were collected, replated, and used as neural progenitor cells. Consistent with the data from WFS1 and WFS2 knockout mice, we observed that spectrin cleavage was increased in neural progenitor cells derived from Wolfram-iPSCs relative to control iPSCs, which indicates increased calpain activity (Fig. 5*G*).

Because calpain is known to be activated by high calcium, we explored the possibility that cytoplasmic calcium may be increased in patient cells by staining neural progenitor cells derived from

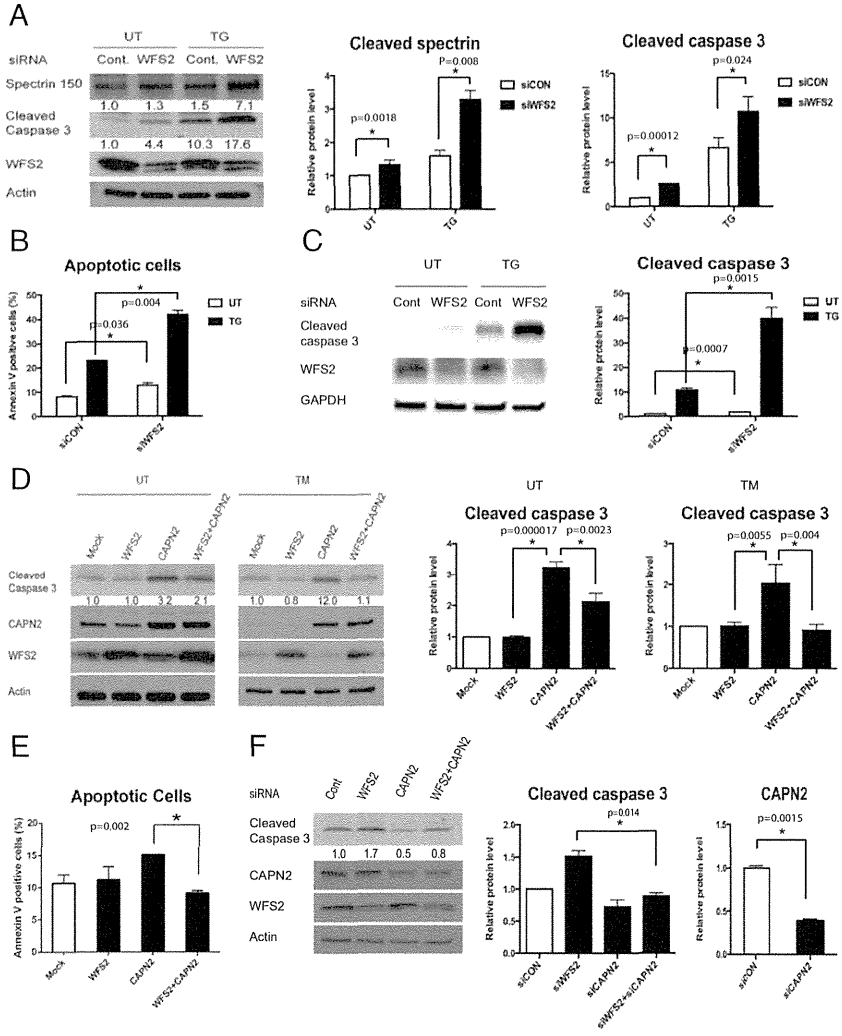

Fig. 2. WFS2 suppresses cell death mediated by CAPN2. (*A*) NSC34 cells were transfected with control scrambled siRNA or siRNA directed against WFS2, and then treated with 0.5μM thapsigargin (TG) for 6 h or untreated (UT). Apoptosis was monitored by immunoblotting analysis of cleaved caspase 3. (*Left*) Protein levels of cleaved spectrin, WFS2, and actin were measured by immunoblotting. (*Right*) Quantifications of cleaved spectrin and cleaved caspase 3 are shown ($n = 5$, $^*P < 0.05$). (*B*) NSC34 cells were transfected with control scrambled siRNA or siRNA directed against WFS2, and then treated with 0.5 μM thapsigargin (TG) for 6 h or untreated (UT). Apoptosis was monitored by Annexin V staining followed by flow cytometry analysis. ($n = 3$, $^*P < 0.05$). (*C*) INS-1 832/13 cells were transfected with control scrambled siRNA or siRNA directed against WFS2, and then treated with 0.5 μM thapsigargin (TG) for 6 h or untreated (UT). (*Left*) Expression levels of cleaved caspase 3, WFS2, and actin were measured by immunoblotting. (*Right*) Protein levels of cleaved caspase 3 are quantified ($n = 3$, $^*P < 0.05$). (*D*) NSC34 cells were transfected with empty expression plasmid (Mock), WFS2 expression plasmid, CAPN2 expression plasmid or cotransfected with WFS1 and CAPN2 expression plasmids. Twenty-four h post transfection, cells were treated with 5 μg/mL tunicamycin (TM) for 16 h or untreated (UT). Apoptosis was monitored by immunoblotting analysis of the relative levels of cleaved caspase 3 (indicated in *Left*). Expression levels of CAPN2, WFS2, and actin were also measured by immunoblotting. Quantification of cleaved caspase 3 levels under untreated (*Center*) and tunicamycin treated (*Right*) conditions are shown as bar graphs. ($n = 5$, $^*P < 0.05$). (*E*) Neuro2a cells transfected with empty expression plasmid (Mock), WFS2 expression plasmid, CAPN2 expression plasmid or cotransfected with WFS1 and CAPN2 expression plasmids were examined for apoptosis by Annexin V staining followed by flow cytometry analysis (*Right*, $n = 3$, $^*P < 0.05$). (*F*) NSC34 cells were transfected with scrambled siRNA (Cont), WFS2 siRNA, CAPN2 siRNA or cotransfected with WFS2 siRNA and CAPN2 siRNA. Apoptosis was detected by immunoblotting of cleaved caspase 3. (*Left*) Protein levels of CAPN2, WFS2 and actin were also shown. (*Right*) Quantification of immunoblotting is shown ($n = 3$, $^*P < 0.05$).

control- and Wolfram-iPSCs with Fura-2, a fluorescent calcium indicator which enables accurate measurements of cytoplasmic calcium concentrations. Fig. 5*H*, *Left*, shows that cytoplasmic calcium levels were higher in Wolfram-iPSC-derived neuronal cells relative to control cells. This result was confirmed by staining these cells with another fluorescent calcium indicator, Fluo-4 (Fig. 5*H*, *Right*). Collectively, these results indicate that loss of function of WFS1 increases cytoplasmic calcium levels, leading to calpain activation.

The results shown above argue that the pathway leading to calpain activation provides potential therapeutic targets for Wolfram syndrome. To test this concept, we elected to focus on modulating cytosolic calcium and performed a small-scale screen to identify chemical compounds that could prevent cell death mediated by thapsigargin, a known inhibitor for ER calcium ATPase. Among 73 well characterized chemical compounds that we tested (Table S3), 8 could significantly suppress thapsigargin-mediated cell death. These were PARP inhibitor, dantrolene, NS398, pioglitazone, calpain inhibitor III, docosahexaenoic acid (DHA), rapamycin, and GLP-1 (Fig. 6*A*). GLP-1, pioglitazone, and rapamycin are FDA-approved drugs and have been shown to confer protection against ER stress-mediated cell death (27, 31–33). Dantrolene is another FDA-approved drug clinically used for muscle spasticity and malignant hyperthermia (34). Previous studies

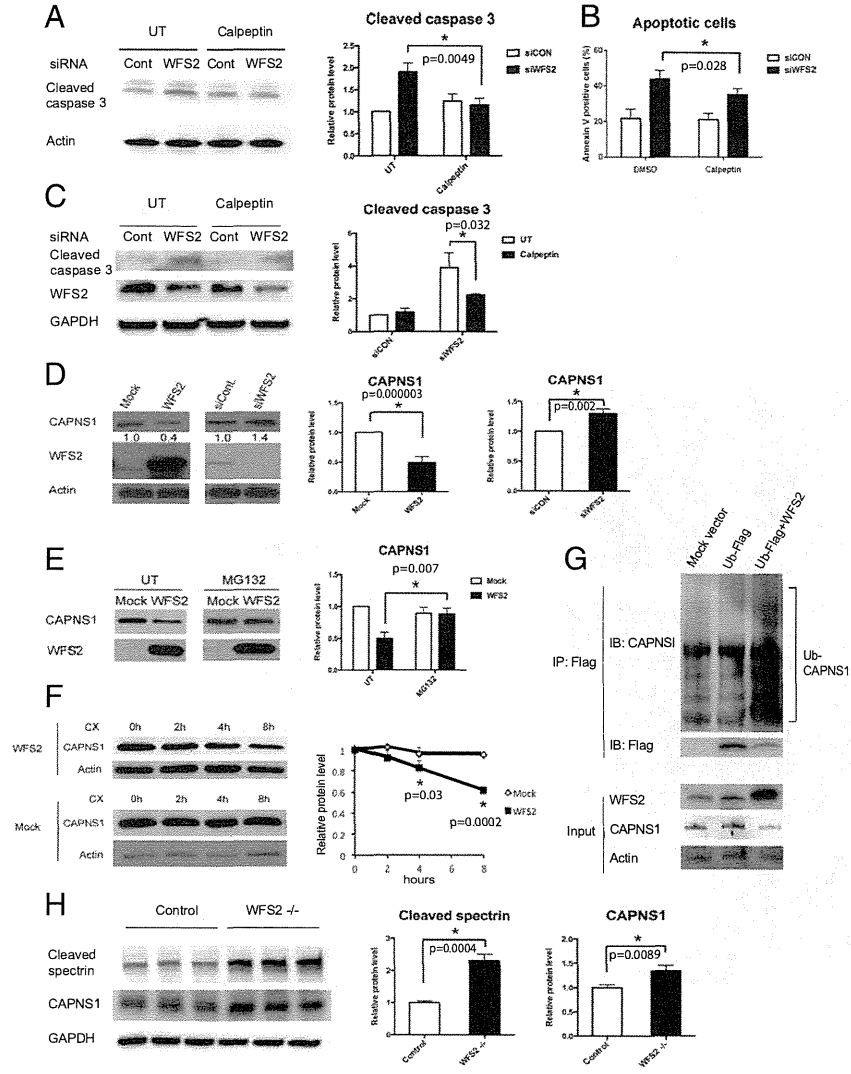

Fig. 3. WFS2 regulates calpain activity through CAPNS1. (*A*) Neuro-2a cells were transfected with siRNA against WFS2 or a control scrambled siRNA. Thirty-six h after transfection, cells were treated with or without 100μM calpeptin for 12 h. Cleaved caspase 3 and actin levels were assessed by immunoblotting (left panel). Cleaved caspase 3 protein levels are quantified in the right panel ($n = 3$, $^*P < 0.05$). (*B*) Neuro-2a cells were transfected with siRNA against WFS2 or scrambled siRNA. Thirty-six h after transfection, cells were treated with or without 100 μM calpeptin for 12 h. Early stage apoptosis was monitored by Annexin V staining followed by flow cytometry ($n = 3$, $^*P < 0.05$). (*C*) INS-1 832/13 cells were transfected with scrambled siRNA and WFS2 siRNA. Twenty-four h after transfection, cells were treated with or without 5 μM calpeptin for 24 h. Cleaved caspase 3, WFS2 and actin levels were monitored by immunoblotting (*Left*) and quantified (*Right*) ($n = 3$, $^*P < 0.05$). (*D*, *Left*) CAPNS1, WFS2, and actin levels were assessed by immunoblotting in HEK293 cells transfected with empty expression plasmid (Mock), WFS2 expression plasmid, scrambled siRNA (siCON), or WFS2 siRNA (siWFS2). (*D*, *Right*) Protein levels of CAPNS1 are quantified ($n = 5$, $^*P < 0.05$). (*E*) HEK293 cells were transfected with empty (Mock) or WFS2 expression plasmid, and then treated with MG132 (2 μM) or untreated (UT). Expression levels of CAPNS1 and WFS2 were measured by immunoblotting (*Left*) and quantified (*Right*) ($n = 4$, $^*P < 0.05$). (*F*) HEK293 cells were transfected with empty or WFS2 expression plasmid, and then treated with cycloheximide (100 μM) for indicated times. (*Left*) Expression levels of CAPNS1 and actin were measured by immunoblotting. (*Right*) Band intensities corresponding to CAPNS1 in *Left* were quantified by Image J and plotted as relative rates of the signals at 0 h ($n = 3$, $^*P < 0.05$). (*G*) NSC34 cells were transfected with mock empty vector, FLAG tagged ubiquitin (Ub-FLAG) plasmid or cotransfected with WFS2 expression plasmid and Ub-FLAG plasmid. Cell lysates were immunoprecipitated with FLAG affinity beads and analyzed for ubiquitin conjugated proteins by immunoblotting. Levels of CAPNS1 and Ub-FLAG protein were measured in the precipitates. WFS2, CAPNS1 and actin expression was monitored in the input samples. (*H*) Brain lysates from control and WFS2 knockout mice were analyzed by immunoblotting. Protein levels of cleaved spectrin and CAPNS1 were determined (*Left*) and quantified (*Center* and *Right*) (each group $n = 3$, $^*P < 0.05$).

have shown that dantrolene is an inhibitor of the ER-localized ryanodine receptors and suppresses leakage of calcium from the ER to cytosol (35, 36). We thus hypothesized that dantrolene could confer protection against cell death in Wolfram syndrome, and performed a series of experiments to investigate this possibility. We first examined whether dantrolene could decrease cytoplasmic calcium levels. As expected, dantrolene treatment decreased cytosolic calcium levels in INS-1 832/13 and NSC34 cells (Fig. S4 *A* and *B*). We next asked whether dantrolene could restore cytosolic calcium levels in WFS1-deficient cells. RNAi-mediated WFS1 knockdown increased cytosolic calcium levels relative to control cells, and dantrolene treatment restored cytosolic calcium levels in WFS1-knockdown INS-1 832/13 cells (Fig. 6*B*, *Left*) as well as WFS1-knockdown NSC34 cells (Fig. 6*B*, *Right*). Next, to determine whether dantrolene confered protection in WFS1-deficient cells, we treated WFS1 silenced INS-1 832/13 cells with dantrolene and observed suppression of apoptosis (Fig. 6*C*) and calpain activity (Fig. 6*D*). Dantrolene treatment also prevented

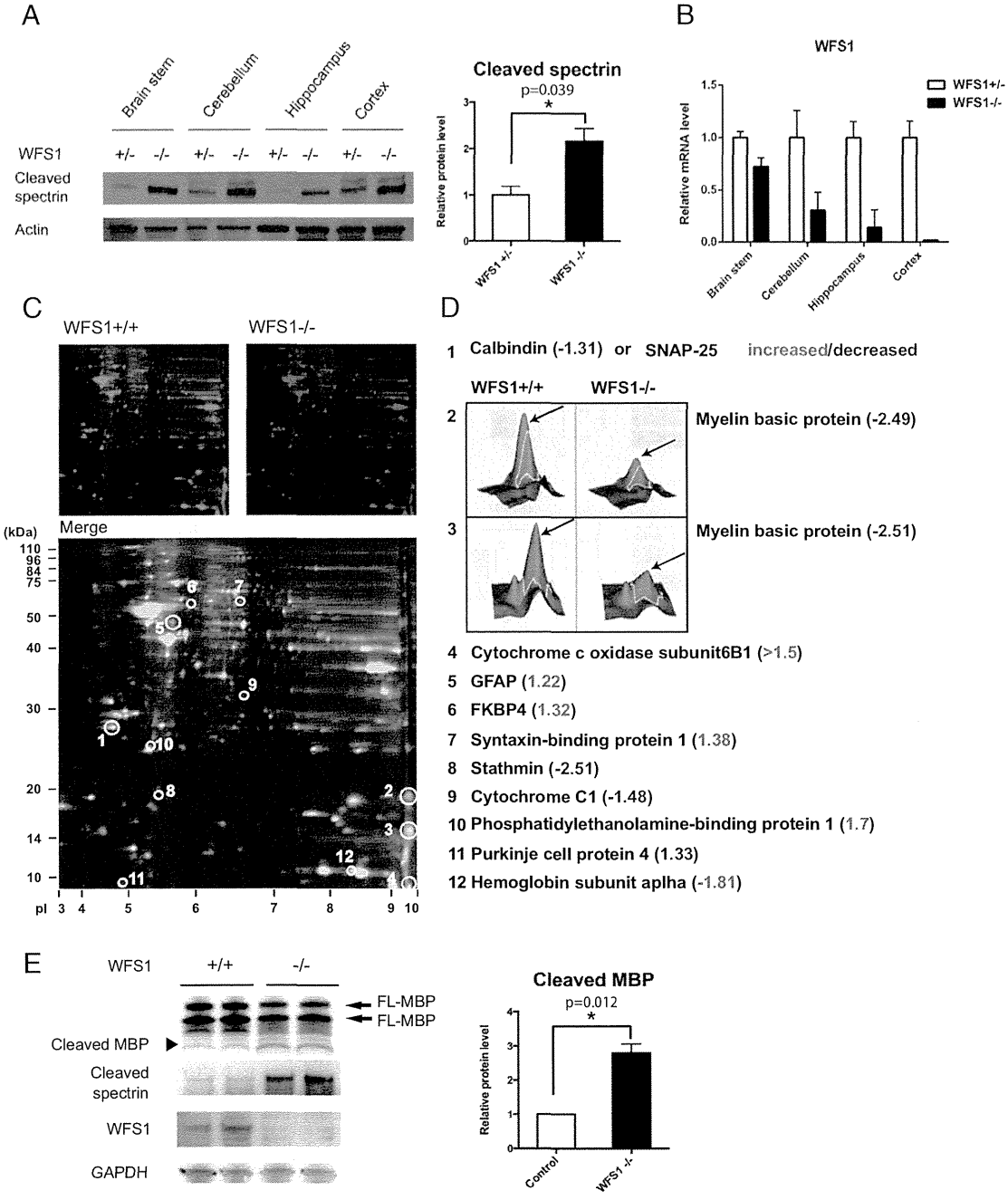

Fig. 4. Evidence of Calpain 2 activation in a mouse model of Wolfram syndrome. (*A*) Protein was extracted from brain tissues of WFS1 brain-specific knockout (–/–) and control (+/–) mice. (*Left*) Cleaved alpha II spectrin and actin levels were determined by immunoblot analysis. (*Right*) Quantification of cleaved spectrin is shown (each group $n = 10$, $^*P < 0.05$). (*B*) WFS1 mRNA levels in different parts of brain in WFS1$^{-/-}$ and WFS1$^{+/-}$ mice were measured by qRT-PCR. (*C*) Two-dimensional fluorescence difference gel electrophoresis of cerebellum proteins from WFS1 knockout (WFS1$^{-/-}$, labeled in red) and control (WFS1$^{+/+}$, labeled in green) mice showing common (Merge, labeled in yellow) and unique proteins (circled). (*D*) The protein expression ratios between WFS1 knockout and control mice were generated, and differentially expressed spots were analyzed by MALDI-TOF mass spectrometry. Quantitative diagrams of spots #2 and #3, identified by mass spectrometry as myelin basic protein, showing lower levels of expression in WFS1 knockout mice compared with control mice. (*E*) Protein was extracted from cerebellums of WFS1 brain-specific knockout (–/–) and control (+/+) mice. Cleaved myelin basic protein (black arrow), cleaved spectrin, WFS1 and GAPDH levels were determined by immunoblot analysis (left panel) and quantified in the right panel (each group $n = 3$, $^*P < 0.05$).

calpain activation and cell death in WFS1-knockdown NSC34 cells (Fig. 6*E*). To verify these observations in patient cells, we pretreated neural progenitor cells derived from iPSCs of a Wolfram syndrome patient and an unaffected parent with dantrolene, and then challenged these cells with thapisgargin. Thapsigargin-induced cell death was increased in neural progenitor cells derived from the Wolfram syndrome patient relative to those derived from the unaffected parent, and dantrolene could prevent cell death in the patient iPSC-derived neural progenitor cells (Fig. 6*F*). In addition, we treated brain-specific WFS1 knockout mice with dantrolene and observed evidence of suppressed calpain activation in brain lysates from these mice (Fig. 6*G*). Collectively, these results argue

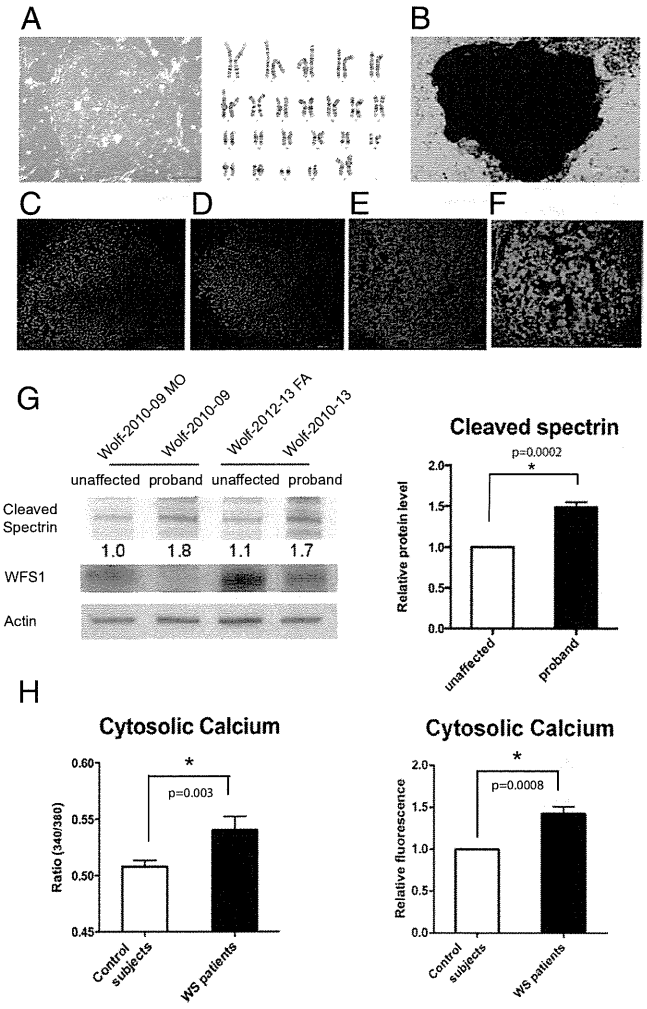

Fig. 5. High cytosolic calcium levels and hyperactivation of calpain in patient neural progenitor cells. (*A, Left*) Wolfram syndrome iPS cells derived from fibroblasts of a patient 1610. (*A, Right*) Karyotype of the Wolfram iPS cells. (*B*) Alkaline phosphatase staining of the Wolfram iPS cells. (*C–F*) Wolfram syndrome iPS cells stained with pluripotent markers: Nanog (*C*), Sox2 (*D*), SSEA4 (*E*), and TRA-1 (*F*). (*G*) Immunoblot analysis of cleaved spectrin and actin in neural progenitor cells derived from Wolfram syndrome patient iPS cells. The relative levels of the spectrin cleavage product are indicated (*Left*) and quantified (*Right*) ($n = 4$, $^*P < 0.05$). (*H, Left*) Quantitative analysis of cytosolic calcium levels in unaffected controls and Wolfram syndrome patients measured by Fura-2 calcium indicator (All values are means ± SEM; experiment was performed six independent times with >3 wells per sample each time; $n = 6$, $^*P < 0.05$). (*H, Right*) Quantification of cytosolic calcium levels in unaffected controls and Wolfram syndrome patients measured by Fluo-4 calcium assay (experiment was performed four independent times; $n = 4$, $^*P < 0.05$).

that dantrolene could prevent cell death in Wolfram syndrome by suppressing calpain activation.

Discussion

Growing evidence indicates that ER dysfunction triggers a range of human chronic diseases, including diabetes, atherosclerosis, inflammatory bowel disease, and neurodegenerative diseases (3, 4, 37–39). However, currently there is no effective therapy targeting the ER for such diseases due to the lack of clear understanding of the ER's contribution to the pathogenesis of these diseases. Although Wolfram syndrome is a rare disease and therefore not a focus of drug discovery efforts, the homogeneity of the patient population and disease mechanism has enabled us to identify a potential target, a calcium-dependent protease, calpain. Our results provide new insights into how the pathways leading to calpain activation cause β cell death and neurodegeneration, which are schematically summarized in Fig. 6*H*.

There are two causative genes for Wolfram syndrome, *WFS1* and *WFS2*. The functions of WFS1 have been extensively studied in pancreatic β cells. It has been shown that WFS1-deficient pancreatic β cells have high baseline ER stress levels and impaired insulin synthesis and secretion. Thus, WFS1-deficient β cells are susceptible to ER stress mediated cell death (5, 6, 32, 40–42). The functions of WFS2 are still not clear. There is evidence showing that impairment of WFS2 function can cause neural atrophy, muscular atrophy, and accelerate aging in mice (14). WFS2 has also been shown to be involved in autophagy (43). However, although patients with both genetic types of Wolfram syndrome suffer from the same disease manifestations, it was not clear if a common molecular pathway was altered in these patients. Our study has demonstrated, to our knowledge for the first time, that calpain hyperactivation is the common molecular pathway altered in patients with Wolfram syndrome. The mechanisms of calpain hyperactivation are different in the two genetic types of Wolfram syndrome. WFS1 mutations cause calpain activation by increasing cytosolic calcium levels, whereas WFS2 mutations lead to calpain activation due to impaired calpain inhibition.

Previously, Wolfram syndrome studies focused on pancreatic β cell function (5, 40, 41). However, patients also suffer from neuronal manifestations. MRI scans of Wolfram syndrome patients showed atrophy in brain tissue implying neurodegeneration in patients (7, 10). To investigate the mechanisms of neurodegeneration in Wolfram syndrome human cells, we established Wolfram syndrome iPSC-derived neural progenitor lines and confirmed the observations found in rodent cells and animal models of Wolfram syndrome. Differentiation of these iPSC-derived neural progenitor cells into specific types of neurons should be carried out in the future to better understand which cell types are damaged in Wolfram syndrome; this will lead to a better understanding of the molecular basis of this disease and provide cell models for future drug development.

Calpain activation has been found to be associated with type 2 diabetes and various neuronal diseases including Alzheimers, traumatic brain injury and cerebral ischemia, suggesting that regulation of calpains is crucial for cellular health (23). We discovered that calpain inhibitor III could confer protection against thapsigargin mediated cell death (Fig. 6*A*). Our data also demonstrates that calpeptin treatment was beneficial for cells with impaired WFS2 function. These results suggest that targeting calpain could be a novel therapeutic strategy for Wolfram syndrome. However, calpain is also an essential molecule for cell survival (44). Controlling calpain activation level is a double-bladed sword. We should carefully monitor calpain functions in treating patients with Wolfram syndrome (44).

Calpain activation is tightly regulated by cytosolic calcium levels. In other syndromes that increase cytosolic calcium level in pancreatic β cells, patients experience a transient or permanent period of hyperinsulinaemic hypoglycemia. This hyperinsulinaemic hypoglycemia can be partially restored by an inhibitor for ATP-sensitive potassium (K_{ATP}) channels or a calcium channel antagonist that prevents an increase in cytosolic calcium levels (45, 46). Although patients with Wolfram syndrome do not experience a period of hyperinsulinaemic hypoglycemia, small molecule compounds capable of altering cellular calcium levels may prevent calpain 2 activation and hold promise for treating patients with Wolfram syndrome. Treatment of WFS1-knockdown cells with dantrolene and ryanodine could prevent cell death mediated by WFS1 knockdown. Dantrolene is a muscle relaxant drug prescribed for multiple sclerosis, cerebral palsy or malignant hyperthermia (47). Dantrolene inhibits the ryanodine receptors and

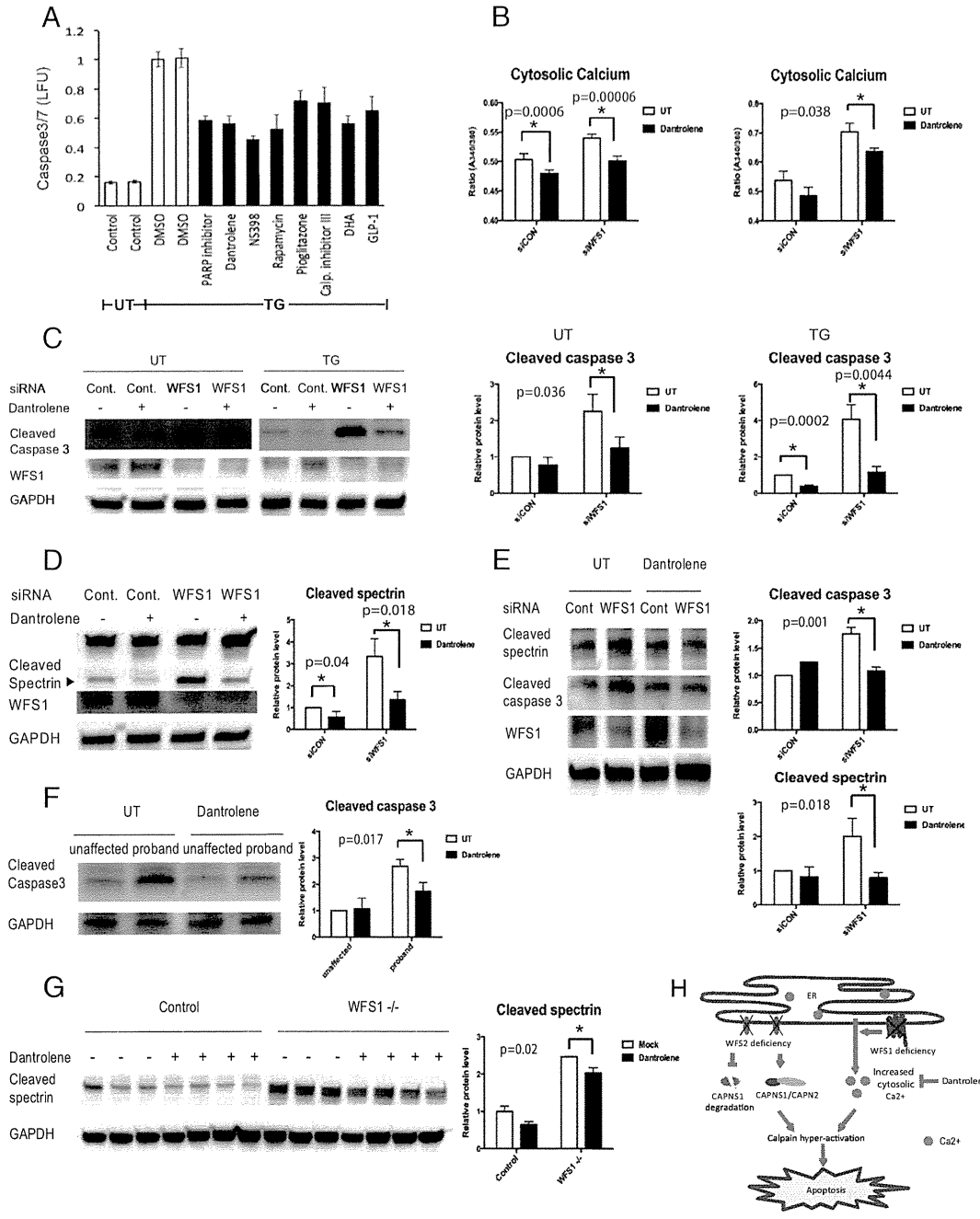

Fig. 6. Dantrolene prevents cell death in iPS cell-derived neural progenitor cells of Wolfram syndorme by inhibiting the ER calcium leakage to the cytosol. (*A*) INS-1 832/13 cells were pretreated with DMSO or drugs for 24 h then incubated in media containing 20 nM of thapsigargin (TG) overnight. Apoptosis was detected by caspase 3/7-Glo luminescence. (*B*) Cytosolic calcium levels were determined by Fura-2 in control and WFS1-deficient INS-1 832/13 (*Left*) and NSC34 (*Right*) cells treated or untreated with 10 μM dantrolene for 24 h (*All* values are means ± SEM; experiment was performed 6 independent times with >3 wells per sample each time $n = 6$, $^*P < 0.05$). (*C*) INS-1 832/13 cells were transfected with scrambled siRNA or siRNA against WFS1. Cells were pretreated with or without 10 μM dantrolene for 48 h, then incubated in media with or without 0.5 μM TG for 6 h. Expression levels of cleaved caspase-3, WFS1, GAPDH were measured by immunoblotting (*Left*). Protein levels of caspase3 under untreated (*Center*) and TG treated (*Right*) conditions are quantified and shown as bar graphs ($n = 3$, $^*P < 0.05$). (*D*) INS-1 832/13 cells were transfected with scrambled siRNA or siRNA against WFS1, pretreated with or without 10 μM dantrolene for 48 h, then incubated in media containing 0.5 μM TG for 6 h. Protein levels of cleaved spectrin, WFS1, GAPDH were analyzed by immunoblotting (*Left*) and quantified (*Right*) ($n = 3$, $^*P < 0.05$). (*E*) NSC34 cells were transfected with scrambled siRNA or siRNA against WFS1. Then treated with or without10 μM dantrolene for 24 h. Protein levels of cleaved spectrin, cleaved caspase 3, WFS2 and GAPDH were determined by immunoblotting (*Left*) and quantified (*Right*) ($n = 3$, $^*P < 0.05$). (*F*) Wolfram patient neural progenitor cells were pretreated with or without 10 μM dantrolene for 48 h. Then, cells were treated with 0.125 μM TG for 20 h. (*Left*) Apoptosis was monitored by immunoblotting. (*Right*) Quantification of cleaved caspase 3 protein levels are indicated ($n = 3$, $^*P < 0.05$). (*G*) Control and WFS1 brain-specific knockout mice were treated with water or dantrolene for 4 wk at 20 mg/kg. Brain lysates of these mice were examined by immunoblotting. Protein levels of cleaved spectrin and GAPDH were monitored (*Left*) and quantified (*Right*) (All values are means ± SEM; each group $n > 3$, $^*P < 0.05$). (*H*) Scheme of the pathogenesis of Wolfram syndrome.

reduces calcium leakage from the ER to cytosol, lowering cytosolic calcium level. The protective effect of dantrolene treatment on WFS1-deficient cells suggests that dysregulated cellular calcium homeostasis plays a role in the disease progression of Wolfram syndrome. In addition, it has been shown that stabilizing ER calcium channel function could prevent the progression of neurodegeneration in a mouse model of Alzheimer's disease (48). Therefore, modulating calcium levels may be an effective way to treat Wolfram syndrome or other ER diseases.

Dantrolene treatment did not block cell death mediated by WFS2 knockdown, suggesting that WFS2 does not directly affect the ER calcium homeostasis (Fig. S4 *D* and *E*). RNAi-mediated WFS1 knockdown in HEK293 cells significantly reduced the activation levels of sarco/endoplasmic reticulum calcium transport ATPase (SERCA), indicating that WFS1 may play a role in the modulation of SERCA activation and ER calcium levels (Fig. S5). It has been shown that WFS1 interacts with the Na^+/K^+ ATPase β1 subunit and the expression of WFS1 parallels that of Na^+/K^+ ATPase β1 subunit in a variety of settings, suggesting that WFS1 may function as an ion channel or regulator of existing channels (42). Further studies on this topic would be necessary to completely understand the etiology of Wolfram syndrome.

Our study reveals that dantrolene can prevent ER stress-mediated cell death in human and rodent cell models as well as mouse models of Wolfram syndrome. Thus, dantrolene and other drugs that regulate ER calcium homeostasis could be used to delay the progression of Wolfram syndrome and other diseases associated with ER dysfunction, including type 1 and type 2 diabetes.

Materials and Methods

Human Subjects. Wolfram syndrome patients were recruited through the Washington University Wolfram Syndrome International Registry website (wolframsyndrome.dom.wustl.edu). The clinic protocol was approved by the Washington University Human Research Protection Office and all subjects provided informed consent if adults and assent with consent by parents if minor children (IRB ID 201107067 and 201104010).

Animal Experiments. WFS1 brain-specific knockout mice were generated by breeding the Nestin-Cre transgenic mice (Jackson Laboratory) with WFS1 floxed mice (40). WFS2 whole body knockout mice are purchased from MRC Harwell. All animal experiments were performed according to procedures approved by the Institutional Animal Care and Use Committee at the Washington University School of Medicine (A-3381-01).

Calcium Levels. Calcium levels in cells were measured by Fura-2 AM dye and Fluo-4 AM dye (Life Technology) Inifinite M1000 (Tecan). Cells were plated in 96-well plates at 25,000 cells per well and stained with 4 μg/mL Fura-2 dye along with 2.5 mM probenecid for 30 min, then the cells were washed with PBS and kept in the dark for another 30 min to allow cleavage of AM ester. Fluorescence was measured at excitation wavelength 510 nm and emission wavelengths 340 nm and 380 nm. Then background subtractions were performed with both emission wavelengths. The subtraction result was used to calculate 340/380 ratios.

For Fluo-4 AM staining, neural progenitor cells were plated in 24-well plates at 200,000 cells per well. After staining with Fluo-4 AM dye for 30 min along with 2.5 mM probenecid, cells were washed and resuspended in PBS. Incubation for a further 30 min was performed to allow complete deesterification of intracellular AM esters. Then, samples were measured by flow cytometry at the FACS core facility of Washington University School of Medicine using a LSRII instrument (BD). The results were analyzed by FlowJo ver.7.6.3.

Statistical Analysis. Two-tailed *t* tests were used to compare the two treatments. *P* values below 0.05 were considered significant. All values are shown as means ± SD if not stated. Please see *SI Materials and Methods* for complete details.

ACKNOWLEDGMENTS. We thank all of the participants in the Washington University Wolfram Registry and Clinic and their families for their time and effort (wolframsyndrome.dom.wustl.edu/). We also thank Mai Kanekura, Mariko Hara, and Karen Sargent for technical support and the Washington University Wolfram Study Group Members and the study staff for advice and support in the greater research program. This work was supported by NIH Grants DK067493, P60 DK020579, and UL1 TR000448; Juvenile Diabetes Research Foundation Grants 47-2012-760 and 17-2013-512; American Diabetes Association Grant 1-12-CT-61, the Team Alejandro, The Team Ian, the Ellie White Foundation for Rare Genetic Disorders, and the Jack and J. T. Snow Scientific Research Foundation (F.U.).

1. Ron D, Walter P (2007) Signal integration in the endoplasmic reticulum unfolded protein response. *Nat Rev Mol Cell Biol* 8(7):519–529.
2. Tabas I, Ron D (2011) Integrating the mechanisms of apoptosis induced by endoplasmic reticulum stress. *Nat Cell Biol* 13(3):184–190.
3. Hetz C, Chevet E, Harding HP (2013) Targeting the unfolded protein response in disease. *Nat Rev Drug Discov* 12(9):703–719.
4. Wang S, Kaufman RJ (2012) The impact of the unfolded protein response on human disease. *J Cell Biol* 197(7):857–867.
5. Fonseca SG, et al. (2005) WFS1 is a novel component of the unfolded protein response and maintains homeostasis of the endoplasmic reticulum in pancreatic beta-cells. *J Biol Chem* 280(47):39609–39615.
6. Fonseca SG, et al. (2010) Wolfram syndrome 1 gene negatively regulates ER stress signaling in rodent and human cells. *J Clin Invest* 120(3):744–755.
7. Barrett TG, Bundey SE, Macleod AF (1995) Neurodegeneration and diabetes: UK nationwide study of Wolfram (DIDMOAD) syndrome. *Lancet* 346(8988):1458–1463.
8. Wolfram DJ, Wagener HP (1938) Diabetes mellitus and simple optic atrophy among siblings: Report of four cases. *Mayo Clin Proc* 1:715–718.
9. Urano F (2014) Diabetes: Targeting endoplasmic reticulum to combat juvenile diabetes. *Nat Rev Endocrinol* 10(3):129–130.
10. Hershey T, et al.; Washington University Wolfram Study Group (2012) Early brain vulnerability in Wolfram syndrome. *PLoS ONE* 7(7):e40604.
11. Marshall BA, et al.; Washington University Wolfram Study Group (2013) Phenotypic characteristics of early Wolfram syndrome. *Orphanet J Rare Dis* 8(1):64.
12. Inoue H, et al. (1998) A gene encoding a transmembrane protein is mutated in patients with diabetes mellitus and optic atrophy (Wolfram syndrome). *Nat Genet* 20(2):143–148.
13. Amr S, et al. (2007) A homozygous mutation in a novel zinc-finger protein, ERIS, is responsible for Wolfram syndrome 2. *Am J Hum Genet* 81(4):673–683.
14. Chen YF, et al. (2009) Cisd2 deficiency drives premature aging and causes mitochondria-mediated defects in mice. *Genes Dev* 23(10):1183–1194.
15. Wiley SE, et al. (2013) Wolfram Syndrome protein, Miner1, regulates sulphydryl redox status, the unfolded protein response, and Ca2+ homeostasis. *EMBO Mol Med* 5(6):904–918.
16. Shang L, et al. (2014) β-cell dysfunction due to increased ER stress in a stem cell model of Wolfram syndrome. *Diabetes* 63(3):923–933.
17. Sandhu MS, et al. (2007) Common variants in WFS1 confer risk of type 2 diabetes. *Nat Genet* 39(8):951–953.
18. Bonnycastle LL, et al. (2013) Autosomal dominant diabetes arising from a Wolfram syndrome 1 mutation. *Diabetes* 62(11):3943–3950.
19. Goll DE, Thompson VF, Li H, Wei W, Cong J (2003) The calpain system. *Physiol Rev* 83(3):731–801.
20. Tan Y, et al. (2006) Ubiquitous calpains promote caspase-12 and JNK activation during endoplasmic reticulum stress-induced apoptosis. *J Biol Chem* 281(23):16016–16024.
21. Tan Y, Wu C, De Veyra T, Greer PA (2006) Ubiquitous calpains promote both apoptosis and survival signals in response to different cell death stimuli. *J Biol Chem* 281(26):17689–17698.
22. Nakagawa T, Yuan J (2000) Cross-talk between two cysteine protease families. Activation of caspase-12 by calpain in apoptosis. *J Cell Biol* 150(4):887–894.
23. Cui W, et al. (2013) Free fatty acid induces endoplasmic reticulum stress and apoptosis of β-cells by Ca2+/calpain-2 pathways. *PLoS ONE* 8(3):e59921.
24. Huang CJ, et al. (2010) Calcium-activated calpain-2 is a mediator of beta cell dysfunction and apoptosis in type 2 diabetes. *J Biol Chem* 285(1):339–348.
25. Barrett TG, Bundey SE (1997) Wolfram (DIDMOAD) syndrome. *J Med Genet* 34(10):838–841.
26. Liu MC, et al. (2006) Comparing calpain- and caspase-3-mediated degradation patterns in traumatic brain injury by differential proteome analysis. *Biochem J* 394(Pt 3):715–725.
27. Hara T, et al. (2014) Calcium efflux from the endoplasmic reticulum leads to β-cell death. *Endocrinology* 155(3):758–768.
28. Takei D, et al. (2006) WFS1 protein modulates the free Ca(2+) concentration in the endoplasmic reticulum. *FEBS Lett* 580(24):5635–5640.
29. Liu MC, et al. (2006) Extensive degradation of myelin basic protein isoforms by calpain following traumatic brain injury. *J Neurochem* 98(3):700–712.
30. Takahashi K, Yamanaka S (2006) Induction of pluripotent stem cells from mouse embryonic and adult fibroblast cultures by defined factors. *Cell* 126(4):663–676.
31. Yusta B, et al. (2006) GLP-1 receptor activation improves beta cell function and survival following induction of endoplasmic reticulum stress. *Cell Metab* 4(5):391–406.
32. Akiyama M, et al. (2009) Increased insulin demand promotes while pioglitazone prevents pancreatic beta cell apoptosis in Wfs1 knockout mice. *Diabetologia* 52(4):653–663.
33. Bachar-Wikstrom E, et al. (2013) Stimulation of autophagy improves endoplasmic reticulum stress-induced diabetes. *Diabetes* 62(4):1227–1237.
34. Dykes MH (1975) Evaluation of a muscle relaxant: Dantrolene sodium (Dantrium). *JAMA* 231(8):862–864.

35. Wei H, Perry DC (1996) Dantrolene is cytoprotective in two models of neuronal cell death. *J Neurochem* 67(6):2390–2398.
36. Luciani DS, et al. (2009) Roles of IP3R and RyR Ca2+ channels in endoplasmic reticulum stress and beta-cell death. *Diabetes* 58(2):422–432.
37. Hotamisligil GS (2010) Endoplasmic reticulum stress and atherosclerosis. *Nat Med* 16(4):396–399.
38. Hotamisligil GS (2010) Endoplasmic reticulum stress and the inflammatory basis of metabolic disease. *Cell* 140(6):900–917.
39. Ozcan L, Tabas I (2012) Role of endoplasmic reticulum stress in metabolic disease and other disorders. *Annu Rev Med* 63:317–328.
40. Riggs AC, et al. (2005) Mice conditionally lacking the Wolfram gene in pancreatic islet beta cells exhibit diabetes as a result of enhanced endoplasmic reticulum stress and apoptosis. *Diabetologia* 48(11):2313–2321.
41. Ishihara H, et al. (2004) Disruption of the WFS1 gene in mice causes progressive beta-cell loss and impaired stimulus-secretion coupling in insulin secretion. *Hum Mol Genet* 13(11):1159–1170.
42. Zatyka M, et al. (2008) Sodium-potassium ATPase 1 subunit is a molecular partner of Wolframin, an endoplasmic reticulum protein involved in ER stress. *Hum Mol Genet* 17(2):190–200.
43. Chang NC, Nguyen M, Germain M, Shore GC (2010) Antagonism of Beclin 1-dependent autophagy by BCL-2 at the endoplasmic reticulum requires NAF-1. *EMBO J* 29(3): 606–618.
44. Dutt P, et al. (2006) m-Calpain is required for preimplantation embryonic development in mice. *BMC Dev Biol* 6:3.
45. Arya VB, Mohammed Z, Blankenstein O, De Lonlay P, Hussain K (2014) Hyperinsulinaemic hypoglycaemia. *Hormone Metabolic Res* 46(3):157–170.
46. Shah P, Demirbilek H, Hussain K (2014) Persistent hyperinsulinaemic hypoglycaemia in infancy. *Semin Pediatr Surg* 23(2):76–82.
47. Krause T, Gerbershagen MU, Fiege M, Weisshorn R, Wappler F (2004) Dantrolene—a review of its pharmacology, therapeutic use and new developments. *Anaesthesia* 59(4):364–373.
48. Chakroborty S, et al. (2012) Stabilizing ER Ca2+ channel function as an early preventative strategy for Alzheimer's disease. *PLoS ONE* 7(12):e52056.

nature COMMUNICATIONS

ARTICLE

Received 24 Jan 2014 | Accepted 2 Oct 2014 | Published 14 Nov 2014

DOI: 10.1038/ncomms6464 OPEN

The role of maternal-specific H3K9me3 modification in establishing imprinted X-chromosome inactivation and embryogenesis in mice

Atsushi Fukuda[1], Junko Tomikawa[2], Takumi Miura[1], Kenichiro Hata[2], Kazuhiko Nakabayashi[2], Kevin Eggan[3], Hidenori Akutsu[1] & Akihiro Umezawa[1]

Maintaining a single active X-chromosome by repressing *Xist* is crucial for embryonic development in mice. Although the *Xist* activator RNF12/RLIM is present as a maternal factor, maternal *Xist* (Xm-*Xist*) is repressed during preimplantation phases to establish imprinted X-chromosome inactivation (XCI). Here we show, using a highly reproducible chromatin immunoprecipitation method that facilitates chromatin analysis of preimplantation embryos, that H3K9me3 is enriched at the *Xist* promoter region, preventing Xm-*Xist* activation by RNF12. The high levels of H3K9me3 at the *Xist* promoter region are lost in embryonic stem (ES) cells, and ES-cloned embryos show RNF12-dependent *Xist* expression. Moreover, lack of Xm-XCI in the trophectoderm, rather than loss of paternally expressed imprinted genes, is the primary cause of embryonic lethality in 70–80% of parthenogenotes immediately after implantation. This study reveals that H3K9me3 is involved in the imprinting that silences Xm-*Xist*. Our findings highlight the role of maternal-specific H3K9me3 modification in embryo development.

[1] Department of Reproductive Biology, National Research Institute for Child Health and Development, 2-10-1 Okura, Setagaya, Tokyo 157-8535, Japan. [2] Department of Maternal-Foetal Biology, National Research Institute for Child Health and Development, 2-10-1 Okura, Setagaya, Tokyo 157-8535, Japan. [3] The Howard Hughes Medical Institute, Harvard Stem Cell Institute and the Department of Stem Cell and Regenerative Biology, Harvard University, 7 Divinity Avenue, Cambridge, Massachusetts 02138, USA. Correspondence and requests for materials should be addressed to H.A. (email: akutsu-h@ncchd.go.jp).

To maintain proper dosage compensation in mammals, one of the two X chromosomes in the female is inactivated[1,2]. In establishment of X-chromosome inactivation (XCI), a large non-coding RNA, *Xist*, is expressed and this non-coding RNA then covers the entire X chromosome in *cis*[1–3]. In mice, two types of XCI occur during female embryonic development. One type involves random XCI, which is observed in cells derived from epiblasts, and one of the two X chromosomes (paternal or maternal) is randomly inactivated. The other involves imprinted XCI (iXCI), which is observed in extra-embryonic tissues and causes XCI of the paternal X chromosome (Xp)[4]. The initiation of iXCI begins at early preimplantation in embryos and Xp-*Xist* is expressed around the four-cell stage[1]. A recent study showed that a maternal factor, the E3 ubiquitin ligase RNF12, is the primary factor responsible for Xp-*Xist* activation[5]. Interestingly, although RNF12 is abundant as a maternal factor in oocytes, Xm-*Xist* is not expressed. Moreover, maternal *Xist* (Xm-*Xist*)-specific imprints, which are refractory to the Xm-*Xist* activation induced by RNF12, are imposed during oogenesis[6]. *Xist* expression analysis using *de novo* DNA methyltransferase (*Dnmt3a/b*) maternal knockout mice demonstrated that *Xist* expression during preimplantation is independent of DNA methylation[7], implying that other epigenetic factors are associated with Xm-*Xist* silencing. However, the nature of these Xm-specific epigenetic modifications is unknown.

A gene-knockout study demonstrated that loss of Xp-*Xist* expression critically affects postimplantation female development due to lack of iXCI, which causes overexpression of X-linked genes in extra-embryonic tissues[8]. Similar to the phenotype observed in Xp-*Xist*-knockout mice, parthenogenetic embryos (PEs) composed of two X chromosomes show increased expression of X-linked genes, as compared with fertilized females, because of the low expression of *Xist*[9]. One of the interesting phenomena observed in PEs is the dramatic developmental failure that occurs immediately after implantation. Around 70–80% of embryos die before embryonic day (E) 9.5, which is the limit of development for PEs[10]. However, it is unknown whether the primary cause of rapid developmental failure in postimplantation PEs is the loss of iXCI or the loss of expression of autosomal paternally imprinted genes[11,12].

The global epigenetic asymmetry of parental genomes in zygotes is retained during early preimplantation phases in mice and changes in gene expression occur in discrete stages to confer totipotency[13,14]. Interestingly, transcriptionally repressive marks, such as histone H3 lysine 9 di-/trimethylation (H3K9me2/3), are specifically imposed on maternal genomes at the zygote stage[13]. Although the regulation of imprinted genes mostly depends on DNA methylation, some imprinted genes are regulated by these histone modifications[15,16]. Thus, Xm-*Xist* silencing machinery may be associated with histone modifications.

Here we reveal that silencing of Xm-*Xist* in preimplantation embryos involves modification of H3K9me3. By using a new chromatin immunoprecipitation (ChIP) method that facilitates chromatin analysis in preimplantation embryos, we show that the *Xist* promoter on the Xm is highly enriched for H3K9me3 at the four-cell stage. This enrichment is lost in the morula and in male embryonic stem (ES) cells. Furthermore, we demonstrate that early loss of H3K9me3 at the *Xist* promoter leads to precocious Xm-*Xist* activation in a Rnf12-dependent manner. Moreover, we demonstrate that establishment of Xm-XCI in the trophectoderm allows PEs to develop at the postimplantation stage without the expression of paternally imprinted genes on autosomes. Therefore, these data indicate that the primary cause of embryonic lethality immediately after implantation in most PEs is loss of XCI rather than loss of the expression of paternally imprinted genes located on autosomes. Our study revealed that silencing of Xm-*Xist* by imprinting to establish iXCI involves H3K9me3, and this finding is expected to resolve the longstanding issues that have limited our general understanding of XCI in mice.

Results

Changes in histone modifications cause Xm-*Xist* derepression. Histone repressive marks, such as H3K9me2/3 and H3K27me3, are specifically imposed on maternal genomes[13]. To investigate the role of maternal-specific modifications in imprinted *Xist* expression, we focused on *Kdm3a* and *Kdm4b*, which encode histone demethylases specific for H3K9me1/2 and H3K9me3 (refs 17,18), respectively. Reverse transcription–PCR analysis showed that oocytes express low levels of *Kdm3a* and *Kdm4b* (Supplementary Fig. 1). Immunofluorescence (IF) analyses revealed that zygotes injected with polyadenylated *Kdm3a* and *Kdm4b* messenger RNAs expressed significantly lower levels of maternal H3K9me2 and H3K9me3, respectively (Fig. 1a–d). Ectopic expression of *Kdm3a* and *Kdm4b* did not affect H3K9me3 or H3K9me2 marks, respectively (Supplementary Fig. 2). We reasoned that if Xm-specific modifications that prevent *Xist* activation were erased by these epigenetic modifiers, Xm-*Xist* would be expressed at the four-cell stage, which is when Xp-*Xist* expression commences.

To facilitate analysis of Xm-*Xist* expression, we used PEs (Fig. 1e). PEs possess two copies of Xm, and Xm-*Xist* is never expressed at the four-cell stage[19]. Xm-*Xist* expression in four-cell PEs, cultured for 48 h, was determined using quantitative real-time PCR (qPCR). Consistent with a previous report[19], Xm-*Xist* was not detectably expressed in most intact (not injected) PEs and PEs injected with *Egfp* mRNA (*Egfp*-PEs; Fig. 1f). Approximately 75% of PEs injected with *Kdm3a* mRNA (*Kdm3a*-PEs) did not detectably express *Xist*. However, Xm-*Xist* expression was detected in all PEs injected with *Kdm4b* mRNA (*Kdm4b*-PEs;

Figure 1 | Alterations in histone modifications derepress Xm-*Xist* expression. (**a**–**d**) Oocytes injected with *Kdm3a* (**a**,**b**), *Kdm4b* (**c**,**d**) or *Egfp* mRNAs were subjected to ICSI. After 7–8 h, embryos were fixed and analysed for H3K9me2 (**a**) and H3K9me3 (**c**) using IF. Nuclei stained with 4′,6-diamidino-2-phenylindole (DAPI) are shown in blue. Representative images are presented on the left. The box-and-whisker plot shows the ratio of maternal to paternal signal intensities. The horizontal line indicates the median. The *P*-values were calculated using the Mann–Whitney *U*-test (*U*-test). Pb, polar body; *n*, number of embryos analysed (**b**,**d**). (**e**) Schema of the generation of PEs with altered histone modifications. To examine the effects of histone demethylation on Xm-*Xist* expression, either H3K9me2 demethylase (*Kdm3a*) or H3K9me3 demethylase (*Kdm4b*) mRNAs were injected into MII oocytes that were then activated. To assess the effects of inhibition of histone deacetylation on Xm-*Xist* expression, oocytes were activated and incubated in the presence of TSA for 24 h. After 48 h, ten four-cell PEs were pooled and analysed as one biological replicate using qPCR. (**f**) Analysis of Xm-*Xist* expression at the four-cell stage. The expression level of Xm-*Xist* in female embryos derived from IVF was defined as 1. One or two asterisks indicate Xm-*Xist* expression in one or two replicates, respectively. The *P*-values were determined using Student's *t*-tests. Error bars indicate the mean ± s.e.m. (**g**–**i**) *Xist* FISH analysis of *Kdm4b*- and *Egfp* + TSA-PEs at the four-cell stage. (**g**) Representative images of FISH results. (**h**) Ratio of cells with *Xist* signal to the total number of cells. *n*, number of interphase cells analysed. (**i**) Ratio of cells with biallelic expression to total cells. The detailed FISH results are shown in Supplementary Table 1. Scale bars, 20 μm.